

# Uspostava ljudskih staničnih linija s endogeno eksprimiranim proteinom tubulinom fluorescentno obilježenim metodom CRISPaint

---

Tintor, Erna

Master's thesis / Diplomski rad

2023

Degree Grantor / Ustanova koja je dodijelila akademski / stručni stupanj: **University of Zagreb, Faculty of Science / Sveučilište u Zagrebu, Prirodoslovno-matematički fakultet**

Permanent link / Trajna poveznica: <https://um.nsk.hr/um:nbn:hr:217:941693>

Rights / Prava: [In copyright](#)/[Zaštićeno autorskim pravom.](#)

Download date / Datum preuzimanja: **2025-03-21**



Repository / Repozitorij:

[Repository of the Faculty of Science - University of Zagreb](#)



UNIVERSITY OF ZAGREB  
FACULTY OF SCIENCE  
DEPARTMENT OF BIOLOGY

Erna Tintor

**Establishment of human cell lines with endogenous expression of  
protein tubulin fluorescently tagged using the *CRISPaint* method**

Master thesis

Zagreb, 2023.

This work was done in the Laboratory of Cell Biophysics, Division of Molecular Biology, Ruđer Bošković Institute, under the mentorship of Prof. Iva Tolić, PhD (Division of Molecular Biology, Ruđer Bošković Institute, 10000 Zagreb, Croatia) and the co-mentorship of Assoc. Prof. Maja Matulić, PhD (Department of Molecular Biology, Faculty of Science, University of Zagreb, 10000 Zagreb, Croatia) This thesis was submitted for review to Department of Biology at Faculty of Science, University of Zagreb in order to achieve the academic degree Master of molecular biology.

## **Acknowledgments**

*Firstly, I would like to express my biggest thanks to my mentor Prof. Iva Tolić, PhD. Thank you for giving me the opportunity to be a part of your group and make my master thesis under your supervision. Working with you has been a great honor.*

*Next, I would like to thank the members of Tolić Group: Jelena, Valentina, Isabella, Ana and Patrik for all the conversations, lunches and cookies we had. Thank you for always being there for me when I needed help and for making me feel like I am truly a part of the team.*

*My deepest gratitude goes to my Iva D. for guiding me through this whole journey, helping me overcome every obstacle and listening to all my thoughts and worries. The completion of this thesis would not have been possible without your immense encouragement.*

*Furthermore, I would like to thank members of Kops group for plasmids and help with the protocol.*

*I would also like to thank my co-mentor Assoc. Prof. Maja Matulić, PhD for all the suggestions and advice in writing this thesis.*

*Moreover, I have to thank all my dear friends for believing in me and being there for me through all these years. Your joy and and perseverance continues to inspire me.*

*I would also like to thank PMF Veslanje for making me stay in good mental and physical shape through rowing.*

*Lastly, I would like to give special thank my family, mom, dad and grandpa for their enormous support. It means the world to me.*

# TEMELJNA DOKUMENTACIJSKA KARTICA

---

Sveučilište u Zagrebu  
Prirodoslovno-matematički fakultet  
Biološki odsjek  
Diplomski rad

## Uspostava ljudskih staničnih linija s endogeno eksprimiranim proteinom tubulinom fluorescentno obilježenim metodom *CRISPaint* Erna Tintor

Rooseveltov trg 6, 10000 Zagreb, Hrvatska

Za promatranje procesa unutar žive stanice, većinom se koristi fluorescencijska mikroskopija. Glavni zahtjev fluorescencijske mikroskopije je to da željeni predmet proučavanja u stanici mora fluorescirati. Jedan od načina za promatranje stanice pod fluorescencijskim mikroskopom je da se stanični proteini obilježe fluorescentnim proteinima. Međutim, egzogeno unešene sekvence za fuzionirane proteine generiraju proteine s neprirodnom razinom ekspresije, a endogeni protein ostaje neobilježen. Endogeno obilježavanje staničnih proteina s fluorescentnim proteinima jedan je od načina za njihovu vizualizaciju bez utjecaja na jačinu ekspresije. Tehnologija CRISPR-Cas (engl. *Clustered Regularly Interspaced Short Palindromic Repeats*) često je korištena u genetičkom inženjerstvu za jednostavno i precizno uređivanje genoma. U ovom radu je korištena novo razvijena metoda *CRISPaint* (engl. *CRISPR-assisted insertion tagging*). To je sustav koji uz pomoć tehnologije CRISPR-Cas omogućava ugradnju gena za fluorescentni protein u genom tj. u ciljanu sekvencu gena, da bi se proizveo endogeni protein obilježen fluorescentnim biljegom. Optimizirala sam protokol za transfekciju uz pomoć plazmida sustava *CRISPaint*-a i uspostavila sam dvije ljudske stanične linije, HeLa i RPE1, s endogeno obilježenim proteinom tubulinom sa zelenim fluorescentnim proteinom. Ove stanične linije se dalje mogu koristiti za promatranje stanične diobe pod fluorescencijskim mikroskopom, a metoda *CRISPaint* se može primijeniti za endogeno obilježavanje i drugih proteina od interesa.

Ključne riječi: HeLa, RPE1, diobeno vreteno, GFP, konfokalna mikroskopija  
(50 stranica, 28 slika, 7 tablica, 68 literaturnih navoda, jezik izvornika: engleski)  
Rad je pohranjen u Središnjoj biološkoj knjižnici

Mentor: prof. dr. sc. Iva Tolić  
Komentor: izv. prof. dr. sc. Maja Matulić

Ocjenitelji:  
izv. prof. dr. sc. Maja Matulić  
prof. dr. sc. Biljana Balen  
izv. prof. dr. sc. Petra Peharec Štefanić

Rad prihvaćen:

## BASIC DOCUMENTATION CARD

---

University of Zagreb  
Faculty of Science  
Department of Biology  
Master thesis

### Establishment of human cell lines with endogenous expression of protein tubulin fluorescently tagged using the *CRISPaint* method

Erna Tintor

Rooseveltovej 6, 10000 Zagreb, Croatia

Fluorescence microscopy is used to observe processes inside a living cell and its main requirement is that the desired object of study in the cell must fluoresce. One way to observe a cell under a fluorescence microscope is to label cellular proteins with fluorescent proteins (FP). However, exogenously introduced sequences for fusion proteins produce proteins with unnatural expression levels while the endogenous protein remains unlabeled. Endogenous labeling of cellular proteins with FP is one way to visualize them without affecting the strength of expression. CRISPR-Cas (Clustered Regularly Interspaced Short Palindromic Repeats) technology is today often used in genetic engineering to simply and precisely edit the genome. In this work, the newly developed method *CRISPaint* (CRISPR-assisted insertion tagging) was used. It is a system that, using CRISPR-Cas technology, enables the incorporation of a gene for FP into the genome in order to produce an endogenous fluorescently tagged protein. I optimized the transfection protocol using *CRISPaint* system plasmids and established two human cell lines, HeLa and RPE1, with endogenously labeled protein tubulin with green FP. These cell lines can be used to observe cell division under a fluorescence microscope and the *CRISPaint* method can be applied for endogenous labeling of other proteins.

Keywords: HeLa, RPE1, mitotic spindle, GFP, confocal microscopy  
(50 pages, 28 figures, 7 tables, 68 references, original in: English)  
Thesis is deposited in Central Biological Library.

Mentor: Prof. Iva Tolić, PhD  
Co-mentor: Assoc. Prof. Maja Matulić, PhD

Reviewers:  
Assoc. Prof. Maja Matulić, PhD  
Prof. Biljana Balen, PhD  
Assoc. Prof. Petra Peharec Štefanić, PhD

Thesis accepted:

## Table of contents

<b>1. Introduction</b>	<b>1</b>
1.1. Microscopy	1
1.1.1. Fluorescence and confocal microscopy	1
1.1.2. Super-resolution microscopy	2
1.1.3. Fluorescent stains	3
1.2. Fluorescent proteins (FP)	4
1.3. Genetic engineering	6
1.4. CRISPR-Cas9	7
1.4.1. Discovery and development of CRISPR system	7
1.4.2. Cas9 structure and modifications	8
1.5. CRISPaint	9
1.6. Microtubule structure	11
1.6.1. The mitotic spindle	12
<b>2. Aims of the study</b>	<b>13</b>
<b>3. Materials and Methods</b>	<b>13</b>
3.1. Materials	13
3.2. Methods	15
3.2.1. Golden Gate assembly	15
3.2.2. Bacterial transformation	19
3.2.3. Plasmid isolation	19
3.2.4. Restriction digestion	20
3.2.5. Plasmid DNA sequencing	21
3.2.6. Cell culture	21
3.2.7. Transfection using FuGENE HD transfection agent	21
3.2.8. Electroporation	24
3.2.9. Fixation and staining	24
3.2.10. Immunofluorescence	25
3.2.11. Confocal microscopy imaging	26
3.2.12. Image analysis	27
<b>4. Results</b>	<b>28</b>
4.1. Establishment of HeLa cell line stably expressing TUBB-TagGFP2	28
4.2. Establishment of RPE1 cell line stably expressing TUBB-TagGFP2	30
4.3. Transfection efficiency	31

4.4. Immunofluorescence images .....	33
4.5. Spindle length and width measurements .....	35
4.6. Transfection trials results .....	37
<b>5. Discussion.....</b>	<b>40</b>
<b>6. Conclusion.....</b>	<b>43</b>
<b>7. Literature.....</b>	<b>44</b>
<b>8. Curriculum vitae .....</b>	<b>52</b>

**List of abbreviations:**

CenA – centromere protein A

Cas9 – CRISPR associated protein 9

CRISPR – clustered regularly interspaced palindromic repeats

CRISPaint – CRISPR-assisted insertion tagging

DSB – double stranded break

GFP – green fluorescent protein

HDR – homology directed repair

HeLa – Henrietta Lacks cervical cancer cell line

NHEJ – non-homologous end joining; cNHEJ - canonical; aNHEJ - alternative

PAM – protospacer-adjacent motif

PuroS – puromycin sensitive

PRC1 – protein regulator of cytokinesis 1

RFP – red fluorescent protein

RPE1 – retinal pigment epithelial cell line

SiR – silicone rhodamine

sgRNA – single guide RNA

STED – stimulated emission depletion

TUBB – tubulin beta chain

# 1. Introduction

## 1.1. Microscopy

Cell size and complexity make it hard to study their structure and functions. That is why one of the most important tools in cell biology is microscopy. Light microscopy is used for both live and fixed cell imaging. For brightfield cell microscopy, live samples usually have to be stained to have visible features while fixed samples are thinly cut so that the light can pass through them. Even then, most cell components are still hard to distinguish. However, better resolution can be achieved with fluorescence microscopy in which cell components can be labelled with probes and dyes of many different colors (Alberts et al., 2017).

### 1.1.1. Fluorescence and confocal microscopy

Fluorescence microscopy is based on the ability of the subject of interest to fluorescence (Kubitscheck, 2017) which can be produced naturally (autofluorescence) or by external fluorescent elements, e.g. using a fluorescent dye (secondary fluorescence). When the specimen is irradiated by excitation light, it is absorbed and re-emitted with lower energy, thus longer wavelength (Kubitscheck, 2017). Due to low and non-specific intrinsic fluorescence of biological molecules, different fluorescent probes and dyes have been developed.

Classic widefield microscopy illuminates the whole sample, but to see only one specific point in a 3D sample it was necessary to find another method for imaging. That led to the development of confocal microscopy in which the sample is illuminated and scanned portion by portion (Sanderson et al., 2014). In a selected depth plane, fluorophores are excited by a narrow beam of laser light. The emission light is then captured by the detectors and the image is displayed on a computer monitor. For this precise scanning, excitation light and the detector have to be in focus and that gave this type of microscopy the name confocal. Introduction of pinholes in the path of the excitation light leads to blocking of all the light that did not come from the region of focus resulting in a clearer image and improved contrast with a greater signal-to-noise ratio (Kubitscheck, 2017) (**Figure 1.**).

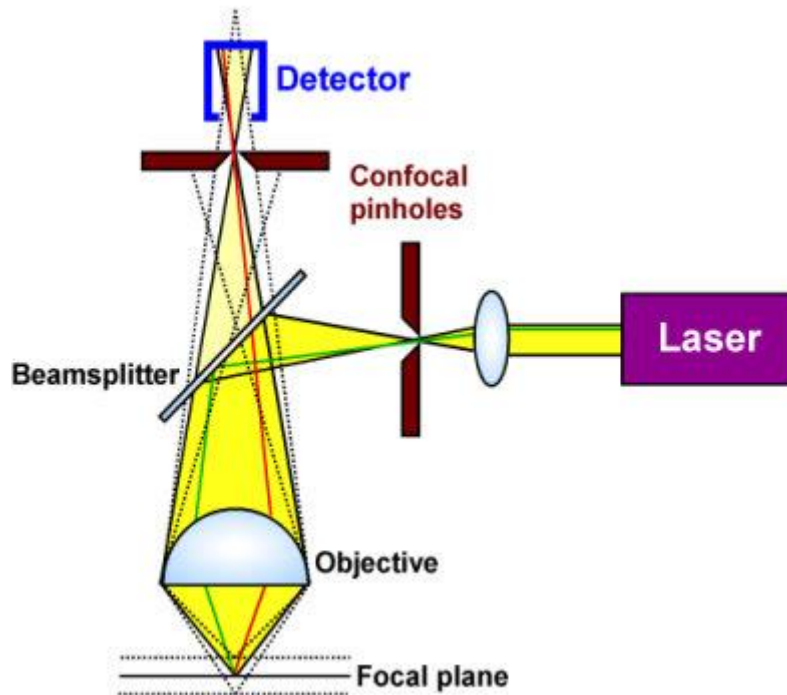


**Figure 1.** Scheme of the confocal microscope. Excitation light comes from the source and passes through confocal pinhole aperture to the sample. The beamsplitter (dichroic mirror) reflects the excitation beam (in green) and splits it from the fluorescence signal (in red). Adapted illustration (Debarnot et al., 2019).

### 1.1.2. Super-resolution microscopy

Regardless of confocal microscopy providing a better image quality than regular fluorescence, a new breakthrough has recently been done with the development of super-resolution microscopy. This method gives us even better resolution without breaking the actual diffraction limit (Sanderson et al., 2014). One example is stimulated emission depletion (STED), in which fluorophores in the outer region of the diffraction limited spot are reversibly silenced - depleted. This is achieved using a second (STED) laser which has a different wavelength (Vicidomini et al., 2018). This allows only nonsilenced fluorophores in the „donut-shaped“ hole to be activated and emit light, resulting in the possibility to separate features closer to the diffraction limit (**Figure 2.**).

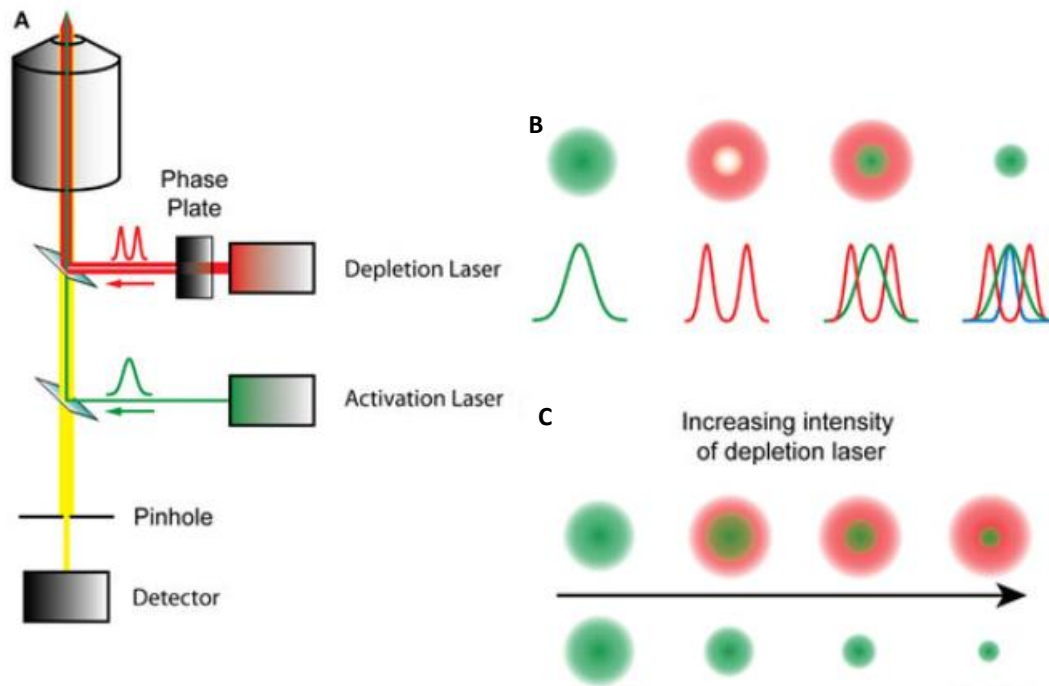


**Figure 2.** Scheme of a STED microscope setup. (A) The activation laser and the depletion laser pass through a phase plate at the same time. A focal point on the sample is excited and emits fluorescence that passes through a pinhole to the detector. (B) At the overlap of the standard fluorescence and the depletion laser, the fluorescence is depleted. Only the fluorescence from the focal point is collected in the detector. (C) When the intensity of the depletion laser increases, the size of the inner ring, the focal point, decreases therefore increasing the resolution. Adapted illustration (Hiersemenzel et al., 2013).

### 1.1.3. Fluorescent stains

Fluorescent stains are usually organic, planar molecules that covalently bond with a functional group or a biomolecule and enable their visualization. These molecules have aromatic rings with delocalized electrons which, after excitation, emit energy - fluorescence (Lichtman & Conchello, 2005). There is a plethora of commercially available fluorescent dyes such as fluorescein isothiocyanate, rhodamine cyanine, and their improved successors such as Alexa Fluor. Another fluorescent stain widely used in both, fixed and live-cell imaging is 4'-diamidino-2-phenylindol, commonly known as DAPI. This stain strongly binds to AT regions of the DNA, absorbs light in the UV and emits light in the blue spectrum (Kapuscinski, 1995). However, it also prone to fading after exposure to UV light (Gallardo-Escárate et al., 2007).

An example of a recent method in labelling microtubules is a taxol-derived fluorescent dye silicone-rhodamine (SiR)-Tubulin. SiR dyes are bright fluorophores that emit in near-infrared range and are quite photostable (Wirth et al., 2019). SiR-Tubulin is very helpful and reliable in microtubule visualization in live imaging (Logan & McCartney, 2020). On the other hand, taxol is known as an antimetabolic agent because it stabilizes microtubules by increasing polymerization and decreasing depolymerization, which results in blocking the cell cycle in G1 or M phase (Arnal & Wade, 1995). Although the probes themselves do not show such strong stabilizing effects on microtubules as taxol, they can still exhibit effects on their structure and stability.

Many of these dyes are used as live cell imaging reagents, but it is necessary to notice that fluorescence imaging of these molecules often produces breakdown products that can be highly cytotoxic (Ettinger & Wittmann, 2014).

## 1.2. Fluorescent proteins (FP)

One of the most important fluorochromes for studying live cells today is green fluorescent protein (GFP) and its variations. GFP was isolated from photoorgans of a jellyfish species *Aequorea victoria* meaning it is a biologically safe fluorophore. This protein is of a specific structure consisting of just 238 amino acids which form a barrel-like structure of beta sheets (Tsien, 1998). In the center of the beta-barrel is a chromophore - molecule responsible for the green color that GFP emits (**Figure 3.**). Since GFP is highly stable and quite small, it exhibits very mild if any effects on the cell (Logan & McCartney, 2020). Moreover, in comparison to organic dyes, the cytoplasm is more protected from reactive free radical breakdown products because the fluorophore is isolated in the fluorescent protein (FP) beta barrel structure (Ettinger & Wittmann, 2014).

Other variations of FP have been developed by mutagenesis of original GFP resulting in cyan and yellow FP as well as a range of FP on the other side of spectrum after the discovery of red fluorescent protein (RFP). Also, FP can be engineered for improved fluorescence, brightness and longer wavelengths. One of the most commonly used variants of GFP is EGFP (enhanced GFP) which has mutations at positions F64L and S65T making it brighter. EGFP also has a shorter maturation time than wild-type GFP (Heim & Tsien, 1996). Using recombinant technology, FP gene can be encoded downstream of the gene of the protein of interest resulting in a fusion protein (Yu et al., 2015). Such gene construct is then transferred into the cell and expressed protein can be observed *in vivo*. One thing to consider is that in this case expression

of the fusion protein is not endogenous and it would be more biologically accurate to have it be expressed endogenously.

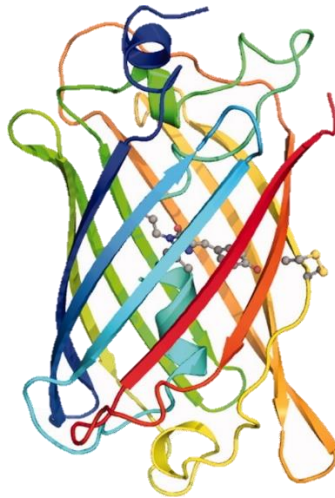


**Figure 3.** Molecular structure of green fluorescent protein. Thick strands are beta sheets, thin strands are alpha loops and in the center is the chromophore (Remington, 2011).

Except from *A. victoria*, FP have also been derived from other organisms, mostly of the *Cnidaria* phylum (Prasher et al., 1992). One such protein is TagGFP2 which originates from *A. macrodactyla* and is a green fluorescent protein that is constitutively fluorescent. In comparison to widely used EGFP, TagGFP2 is brighter, has a much shorter maturation time and lower acid sensitivity. Besides that, TagGFP2 has a larger Stokes shift - the gap between the excitation and emission maxima (Heim & Tsien, 1996), which means that its self-absorption is lower as well as higher extinction coefficient resulting in more energy absorbed and available for emission (**Figure 4.**). TagGFP2 amino acid sequence is shown in **Figure 5.**

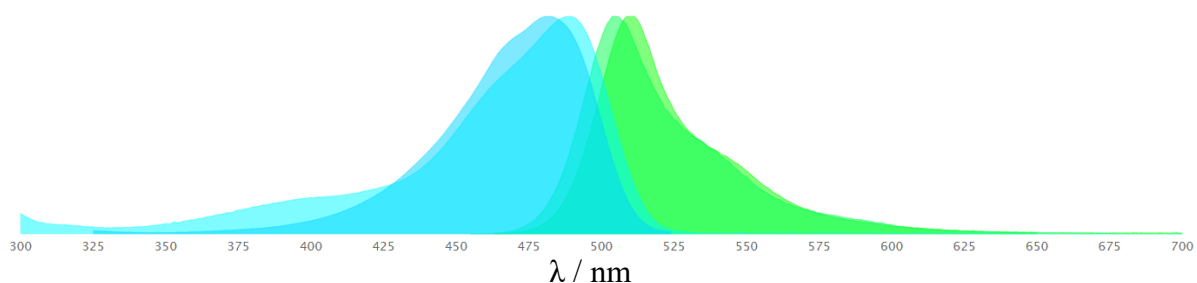


**Figure 4.** Excitation and emission spectrums of EGFP (blue) and TagGFP2 (green). Image obtained and adapted from <https://www.fpbases.org/protein/taggfp2/> ).

```
1  MSGGEELFAG  IVPVLIELDG  DVHGHKFSVR  GEGEDADYD  KLEIKFICTT
51  GKLPVPWPTL  VTTLCYGIQC  FARYPEHMKM  NDFFKSAMPE  GYIQERTIQF
101 QDDGKYKTRG  EVKFEGDTLV  NRIELKGKDF  KEDGNILGHK  LEYSFNSHNV
151 YIRPDKANNG  LEANFKTRHN  IEGGGVQLAD  HYQTNVPLGD  GPVLIPINHY
201 LSTQTKISKD  RNEARDHML  LESFSACCHT  HGMDLYR
```

**Figure 5.** Amino acid sequence of TagGFP2 protein. Image obtained and adapted from <https://www.fpbase.org/protein/taggfp2/> .

### 1.3. Genetic engineering

Genetic engineering uses biotechnological tools to insert or delete nucleotides of genomic DNA, meaning the genome can be manipulated to make new combinations of genetic material which can be inherited. Early technologies that enabled precise manipulation of eukaryotic genes were ZFNs (Zinc-Finger Nucleases) and TALENs (Transcription Activator-Like Effector Nucleases). ZFNs have a zinc-finger domain which recognizes a specific 9 – 18 bp long target sequence and binds to it. Then, endonuclease domain FokI recognizes zinc-finger domain and cuts the DNA strand at that spot, making a double stranded break (DSB) (Carroll, 2011). TALENs, on the other hand, are proteins consisting of TAL effector DNA binding domain which consist of 33 – 35 repeating amino acid sequences that are highly conserved (Joung & Sander, 2013). These amino acid sequences have two variable positions which are responsible for specific nucleotide recognition and that allowed for the construction of precise DNA-binding domains. Upon DNA-binding, FokI domain is activated and makes a DSB which can then be repaired via non-homologous end joining (NHEJ) or homology-directed repair (HDR). NHEJ is considered prone to mistakes and often results in point-mutations (insertions or deletions - indels) which can lead to frameshifts and gene knockouts. HDR uses sister chromatid or exogenous complementary DNA as a template which allows for insertion of complete genes in the position of a DSB. One of the drawbacks of these two technologies is that, because of their size and complexity, such domains and repeating sequences can be challenging to construct. Moreover, TALENs are sensitive to DNA methylation and ZFNs can be quite imprecise when it comes to making a DSB. That is why the discovery of CRISPR/Cas (clustered regularly interspaced short palindromic sequences) system made a revolution in genetic engineering (Gaj et al., 2013).

## 1.4. CRISPR-Cas9

### 1.4.1. Discovery and development of CRISPR system

Bacteria have always been an important organism for scientific research and pioneers in the whole genome sequencing because of their relatively small genome. One such research that investigated a part of *Escherichia coli* chromosome found an interesting structure consisting of series of short direct repeats interspaced with short sequences (Ishino et al., 1987). Other bacteria were later found to contain similar repeats and today they are known as clustered regularly interspaced short palindromic sequences (CRISPR). Together with CRISPR-associated (Cas) proteins they create a system that provides acquired bacterial immunity against foreign DNA. During infection, bacteria cut pathogen DNA into fragments and incorporate them into CRISPR locus inside their own genome. These DNA fragments make protospacers that interspace the palindromic sequences of this locus. After this locus is transcribed and processed into CRISPR RNA (crRNA) and *trans*-activating crRNA (tracrRNA), they guide the cleavage of pathogenic DNA by Cas endonucleases (Xu & Li, 2020). The crRNA recognizes target DNA sequence only if it is associated with protospacer adjacent motif (PAM). PAM is a 2-5 bp sequence directly downstream of the target sequence (Gleditzsch et al., 2019) and it defines the location of the cut precisely 3 nucleotides upstream of the PAM sequence (Karvelis et al., 2015).

In the Type II CRISPR/Cas system (**Figure 6.**), crRNA anneals to *trans*-activating crRNAs (tracrRNA), which recognizes 20-bp DNA target and utilizes Cas9 protein to make a DSB. While there are different PAM requirements for a precise cut, one of the systems optimized for genetic engineering relies on *Streptococcus pyogenes* derived 5'-NGG-3' PAM that precedes the target DNA. To further optimize this system for mammalian cells, crRNA and tracrRNA can be fused together to create single-guide RNA (sgRNA). By redesigning sgRNA, virtually any DNA sequence can be targeted for cleavage. CRISPR/Cas9 has since allowed for relatively simple creation of eukaryotic cells bearing precise mutations made by NHEJ and HDR (Ran et al., 2013).

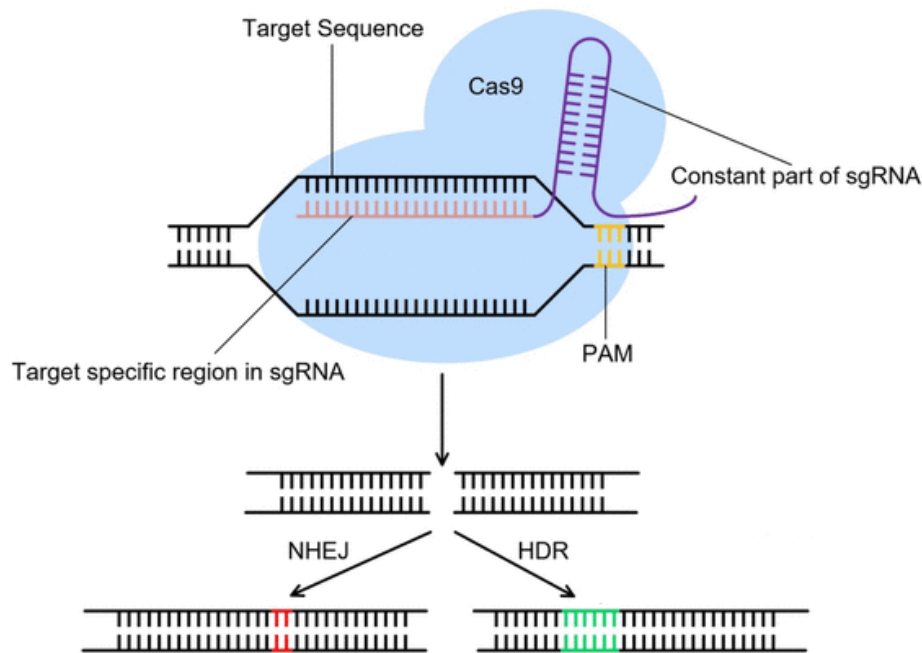


**Figure 6.** CRISPR/Cas9 system. Target sequence is recognized by sgRNA. Cas9 cuts both strands of target DNA upstream of the PAM sequence and DSB is then repaired via NHEJ or HDR pathway (Cui et al., 2018).

### 1.4.2. Cas9 structure and modifications

All Cas9 proteins share a common structure of two distinct parts, REC and NUC. REC is constituted of three alpha-helix domains: Hel-I, Hel-II and Hel-III or REC1, REC2 and REC3, respectively which play a role in binding sgRNA. NUC consists of HNH (histidine-asparagine-histidine nuclease) and RuvC (Rnase H-like) nuclease domains and a C-terminal domain that recognizes PAM sequence. After sgRNA finds the target sequence and Cas9 recognizes PAM sequence, HNH domain cuts the strand complementary to the sgRNA (target strand) and RuvC domain cuts the non-target strand (Jiang & Doudna, 2017).

Above mentioned HNH and RuvC domains can also be mutated for modified function to execute specific cleavages. One such mutation is aspartate-to-alanine (D10A) mutation in the catalytic domain of RuvC which transforms Cas9 into a nickase that makes a single-stranded break. This type of cleavage is preferably repaired through HDR which may decrease the potential for unwanted indel mutations. REC domains can also be modified to reduce or completely eliminate nuclease activity of Cas9 creating its deactivated form (dCas9) (Nishimasu et al., 2014). One example of utilizing dCas9 is that it can be mutated and repurposed as a transcriptional regulator (Qi et al., 2013). Without nuclease activity, dCas9 can

also, for example, be fused with an enzyme that converts one base to another thus making a highly precise point mutation (Komor et al., 2016). Also, dCas9 can be fused with a fluorescent protein to temporarily visualize desired regions in the genome by targeting them with sgRNA-dCas9-FP complex (Dreissig et al., 2017). These examples opened a whole new spectra of possibilities for genetic manipulation via CRISPR/Cas9 system.

## 1.5. CRISPaint

Aforementioned DSB repair pathways, HDR and NHEJ are both used in CRISPR/Cas9 engineering. More challenging gene insertion is usually accomplished using HDR by integrating a DNA fragment with homology arms into the genome while indel mutagenesis is mediated by NHEJ which can proceed into two pathways. The first one is canonical NHEJ (cNHEJ) which repairs DSB by utilizing ligase-4 with minimal or no modification to the dsDNA ends. More recently described alternative NHEJ (aNHEJ) pathway is applied when cNHEJ is disabled and repairs DSB using microhomologies (Chiruvella et al., 2013). Although microhomologies can also be associated with cNHEJ, they are more frequent in aNHEJ pathways.

To insert foreign DNA using HDR, it has to be constructed with homologous regions which can be challenging and in the absence of homologous template HDR pathway is largely less efficient than NHEJ pathway (Iliakis et al., 2004). Furthermore, HDR only occurs while cells are in the S phase (Essers et al., 2002), while NHEJ pathway is active during the whole cell cycle (Hustedt & Durocher, 2017). Albeit it was previously suggested that NHEJ can be prone to indels, cNHEJ is not fundamentally defective. Instead of depending on cNHEJ machinery, the accuracy of end joining is in fact defined by the structure of the DNA ends and cNHEJ adapts the repair accordingly (Bétermier et al., 2014). While the DNA ends may look different for some DSBs, Cas9 makes a precise DSB leaving directly ligatable DNA ends resulting in highly accurate NHEJ (Guo et al., 2018). This is why development of a system that integrates foreign DNA via cNHEJ would provide a simple and modular way for targeted genome engineering. Schmid-Burgk et al. (2016) used such approach to establish a new system for gene tagging: *CRISPaint* (CRISPR-assisted insertion tagging) that relies on cNHEJ. This is a HDR-independent modular method for integrating exogenous genetic material into genomic locations of interest. Precisely, *CRISPaint* is used to tag endogenous genes and generate C-terminally tagged fusion proteins allowing their visualization and quantification in microscopy of live cells

(Schmid-Burgk et al., 2016). This system consists of three plasmids that are simultaneously introduced to the cell (**Figure 7**).

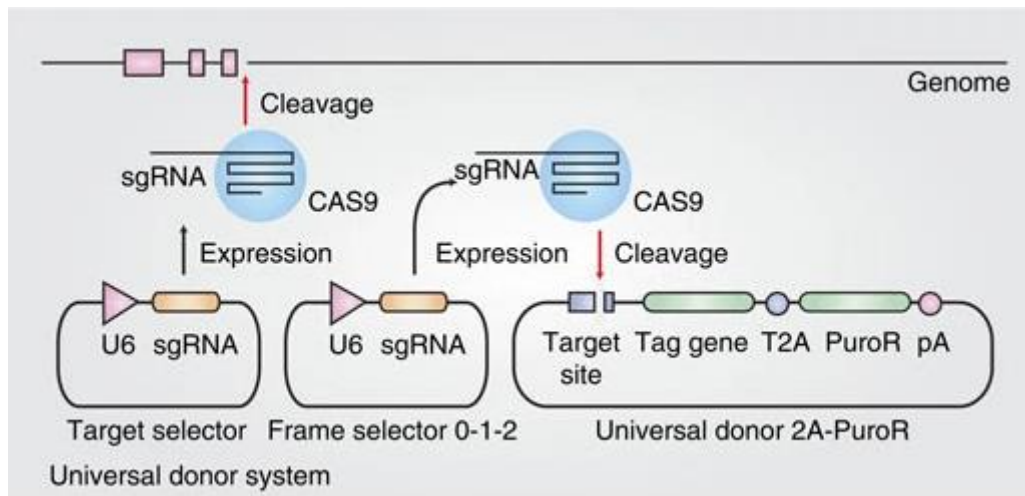


**Figure 7.** Scheme of the *CRISPaint* system with three plasmids. Expression of sgRNAs is under control of the U6 promotor. A universal donor plasmid delivers a tag gene and a puromycin resistance gene, which are separated by a T2A self-cleaving peptide that ensures individual expression. A frame selector cuts the donor plasmid in a way that ensures tag integration in the right frame. Adapted illustration (Schmid-Burgk et al., 2016).

Target selector plasmid contains Cas9 protein and sgRNA that determines the location of a DSB in the genome and universal donor plasmid has a short linker peptide (GGSGGSGGGS) in frame with the tag gene. The sgRNA of the target selector is designed to target the end of the last exon of the protein of interest. Precise cleavage location in the genome is determined by an endogenously existing 5'-NGG-3' PAM sequence downstream of sgRNA complementary sequence and the cut is executed 3 nucleotides upstream of PAM. Considering that PAM could define a cut in between two nucleotides that define a single amino acid, it is important to compensate for a possible loss of one or two nucleotides. For that reason, the frame selector plasmid can compensate by cutting the linker peptide in donor plasmid to ensure that the inserted tag is expressed in the correct reading frame (Schmid-Burgk et al., 2016). For that reason, the right frame has to be chosen for every protein of interest based on their target selector. After the donor plasmid is cleaved, it is linearized and integrated into the genome via NHEJ (Schmid-Burgk et al., 2016).

## 1.6. Microtubule structure

Microtubules are the major component of the eukaryotic cytoskeleton, along with intermediate and actin filaments. In the interphase, microtubules make up a network involved in intracellular transport, motility and cell shape maintenance, while during mitosis they are crucial for executing cell division (Wade, 2009). They are polymers of a tubulin heterodimer which consists of  $\alpha$  and  $\beta$ -tubulin 55 kDa monomers (**Figure 8.A**). Microtubule is formed of 13 parallel protofilaments (**Figure 8.B**) making a cylinder shape approximately 25 nm in diameter (**Figure 8.C**). Tubulin subunits always stack into protofilaments in the same direction, meaning that the  $\beta$ -tubulin subunit of one heterodimer is interacting with the  $\alpha$ -tubulin subunit of the next heterodimer. Considering the dissociation properties of the ends of a microtubule, there is a positive ( $\beta$ -tubulin) and negative ( $\alpha$ -tubulin) end. Plus end is more dynamic with rapid changes between growing and shortening phases, but (de)polymerizations happen on both ends. These properties are driven by chemical energy released from GTP to GDP hydrolysis at the  $\beta$ -tubulin subunit (Alberts et al., 2017). Nucleating location of microtubules in the cell is at the microtubule organizing center (MTOC) otherwise known as the centrosome. The minus end of the microtubule remains attached to the centrosome and the plus end extends into the cell (Wade, 2009). While microtubules are more stable when they are a part of interphase cytoskeleton, they become highly dynamic during mitosis (Alberts et al., 2017).

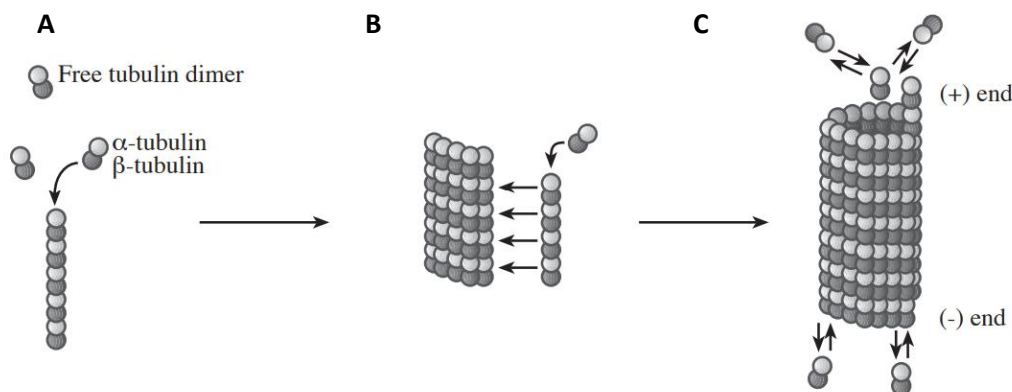


**Figure 8.** Scheme of the microtubule assembly process. (A) Tubulin heterodimers composed of  $\alpha$  and  $\beta$ -tubulin first form protofilaments. (B) 13 protofilaments assemble to form a single microtubule (C) that can shrink or grow via (de)polymerization. Adapted illustration (Borkholder, 1998).

### 1.6.1. The mitotic spindle

Cell division in eukaryotes is performed by the mitotic spindle, a microtubule-built machine responsible for correct segregation of chromosomes into two daughter cells (Walczak & Heald, 2008). The mitotic spindle has a characteristic and precisely defined arrangement of microtubules originating from centrosomes - two orthogonally placed centrioles encased in an amorphous mass. During cell division, centrosomes are positioned at the poles of the spindle making it bipolar. In the center of the spindle, microtubules attach to centromere regions of chromosomes via kinetochores - large multi-protein structures assembled at the surface of the centromere (Musacchio & Desai, 2017).

Most microtubules of the mitotic spindle originate from the poles and are organized in larger structures called bundles. In the center of the spindle, microtubules from the opposite poles overlap, forming antiparallel bundles, are called interpolar microtubules or bridging fibers. Microtubules that stretch from the poles to the cell cortex are called astral microtubules and those which attach to the kinetochores are called kinetochore microtubules or k-fibers (**Figure 9**). One of the essential kinetochore proteins is centromere protein A (CenpA), a histone H3-like variant which plays a major role in kinetochore assembly and chromosome stability (Valdivia et al., 2009).

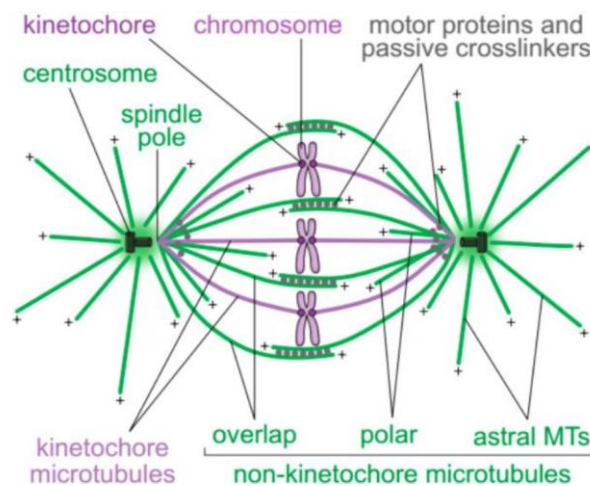


**Figure 9.** Components of the mitotic spindle. Kinetochore microtubules attach to the chromosomes via kinetochores. Non-kinetochore microtubules overlap at the center of the mitotic spindle (overlap), grow from the centrosome towards the center (polar) and the cell cortex (astral), (Tolić, 2018).

Microtubules also interact with microtubule associated proteins (MAPs) which help to create the spindle and support its proper function. MAPs include non-motor and motor proteins like kinesin and dynein that are involved in spindle dynamics (Goodson & Jonasson, 2018). One of the non-motor MAPs is protein regulator of cytokinesis 1 (PRC1) which ensures steady overlaps of the antiparallel microtubules. This activity of PRC1 provides stable microtubule organization and successful progression through anaphase (Jagrić et al., 2021). Astrin or Sperm-associated Antigen 5 (SPAG5) is another MAP, responsible for proper chromosome segregation by maintaining secure kinetochore-microtubule attachments (Ying et al., 2020).

To study the dynamics of the mitotic spindle machinery and chromosome segregation, it is important to observe the cell division under the microscope. Fluorescent dyes and probes are of great help to visualize the most important structures involved in the mitosis.

## **2. Aims of the study**

The goal of this study is to establish cell lines that endogenously express TagGFP2 tagged protein tubulin. One will be non-tumor cell line and the other one a tumor cell line. For that purpose, I will use RPE1 and HeLa cells, respectively. I will establish a protocol for transfection using the *CRISPaint* three-plasmid system. To evaluate the established cells lines, I will measure the parameters of the mitotic spindle. I will also try to establish both cell lines with fluorescently tagged PRC1, Astrin and CenpA which are all proteins of interest in studying mitosis. I will observe and image the cells on a confocal microscope.

## **3. Materials and Methods**

### **3.1. Materials**

#### **Kits:**

QIAprep Spin Miniprep Kit (Cat. No. 27106 QIAGEN GmbH, Hilden, Germany); NucleoBond Xtra Midi plus EF (MACHEREY-NAGEL, GmbH & Co. KG, Düren, Germany); Amaxa Cell Line Nucleofector Kit R (Lonza, Basel, Switzerland)

### **Bacterial culture:**

Liquid Luria-Bertani (LB) medium (in 1 L of dH<sub>2</sub>O): 5 g yeast extract

10 g tryptone

10 g NaCl (10 g)

TSB (transformation/storage buffer, 20 mL): 2 g PEG 3350 (polyethylene glycol)

1 mL DMSO (dimethylsulfoxide)

200 µL MgSO<sub>4</sub> (1M)

200 µL MgCl<sub>2</sub> (1M)

### **Plasmids:**

pKL114-CRISPaint (gift from Kops Lab, Hubrecht Institute, Utrecht, Netherlands)

pCas9-mCherry-TubB (66942; Addgene, Watertown, MA, USA)

pCRISPaint-TagGFP2-PuroR (80970; Addgene, Watertown, MA, USA)

pCas9-mCherry-Frame+0,+1,+2 (66939,66940,66941; Addgene, Watertown, MA, USA)

pCRISPaint-TagRFP-PuroR (80971; Addgene, Watertown, MA, USA)

### **Enzymes and buffers:**

BbsI-HF (R3539S), BsaI-HF (R3733S), CutSmart® Buffer, T4 DNA ligase (M0202S) - (New England Biolabs, Ipswich, USA)

10X Thermo Scientific Tango Buffer (with BSA), dNTP Mix (10 mM each) Cat. No. R0191, ATP Solution (100 mM) Cat. No. R0441, TriTrack DNA Loading Dye (6X) Cat. No. R1161, GeneRuler DNA Ladder Mix Cat. No. SM0331, SYBR™ Safe DNA Gel Stain Cat. No. S33102 - (Thermo Fisher Scientific Inc., Waltham, USA)

Phosphate-buffered saline (PBS; ROTI®Cell PBS CELLPURE®, Carl Roth, Karlsruhe, Germany)

### **Cell lines:**

HeLa mCherry-CenpA (obtained from the lab)

Rpe1 purossensitive (gift from Holland Lab, Johns Hopkins University, USA)

## **Transfection:**

FuGENE<sup>®</sup> HD Transfection Reagent (Promega Corporation, Madison, WI, USA)

Opti-MEM<sup>™</sup> Reduced Serum Medium (Thermo Fisher Scientific Inc., Waltham, USA)

Cell Line Nucleofector<sup>™</sup> Kit L (Lonza, Basel, Switzerland)

## **Immunocytochemistry:**

Fixation solution: 8 mL PFA (paraformaldehyde)

2 mL PBS

50  $\mu$ L glutaraldehyde

Cytoskeleton extraction buffer (CEB):

0,5 % (w/v) Triton X-100

0,1M PIPES (1,4-piperazinediethanesulfonic acid) pH 7

2 mM EDTA (ethylenediaminetetraacetic acid)

1 mM MgCl<sub>2</sub>

## **3.2. Methods**

### **3.2.1. Golden Gate assembly**

Golden Gate assembly is a cloning method in which one or more DNA fragments can be assembled and ligated with a plasmid. The assembly occurs in a single reaction using the activities of Type IIS restriction enzyme and T4 ligase. First step of Golden Gate assembly was to design oligos for sgRNA of interest in a cloud-based platform Benchling (Benchling Inc., San Francisco, CA, USA). Three oligos were designed, targeting proteins important for studying the dynamics of cell division: Astrin, PRC1 and CenpA (**Table 1.**). Mixture for annealing consisted of 1  $\mu$ L forward oligo (100  $\mu$ M), 1  $\mu$ L reverse oligo (100  $\mu$ M) and 8  $\mu$ L nuclease-free dH<sub>2</sub>O (NFW) for every sgRNA. Cycle protocol consisted of incubation for 30 minutes at 37 °C, then for 5 minutes at 97 °C and final step was to lower the temperature by 5 °C every 5 minutes, until the temperature reached 25 °C. Mixture was incubated in a PCR machine. The fragment was inserted in the pKL114-CRISPaint plasmid (**Figure 9. A**) that has a sgRNA scaffold and ampicillin (Amp) resistance gene. The mixture for the Golden Gate Assembly reaction is shown in **Table 2.**

**Table 1.** Sequences of oligos – sgRNAs for annealing.

sgRNA	Sequence (5'-3')
Astrin	F - CACCGCAAAGAAGTACAGGGATTGC R - AAACGCAATCCCTGTAGTTCTTTGC
PRC1	F - CACCGTGATCAGGGCTTCTCAGGAC R - AAACGTCCTGAGAAGCCCTGATCAC
CenpA	F - CACCGCGGGGCCTTGAGGAGGGACT R - AAACAGTCCCTCCTCAAGGCCCCGC

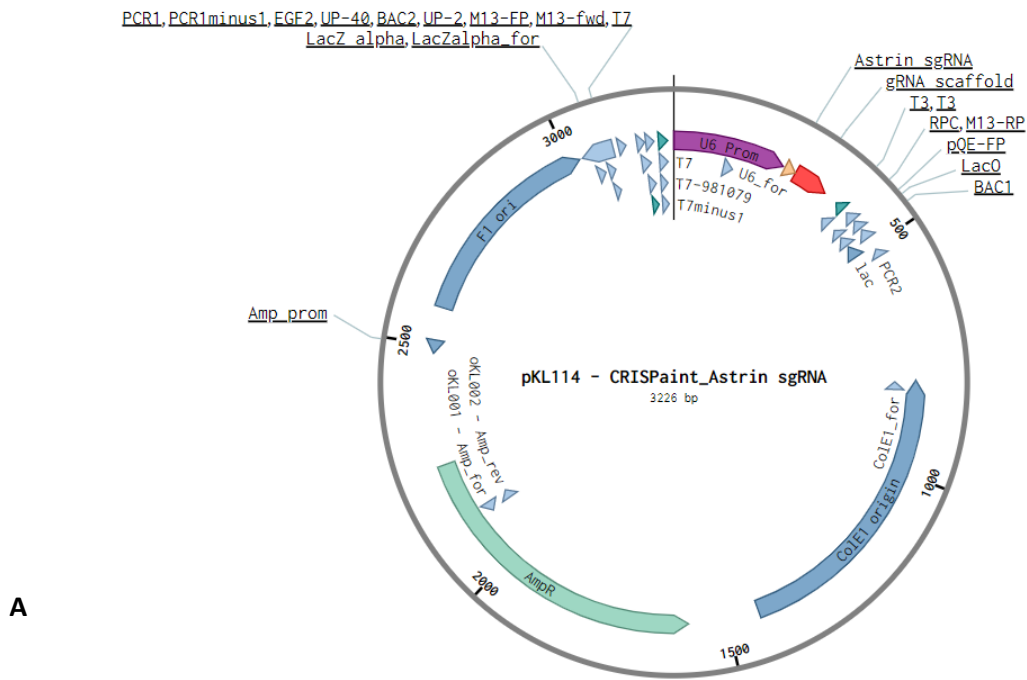
**Table 2.** The reaction mixture for Golden Gate assembly using BbsI-HF restriction enzyme.

Reactants	Volume
Nuclease-free dH <sub>2</sub> O	11,5 µL
Tango buffer (1x)	2 µL
Annealed oligos 1/200	2 µL
pKL114 50 ng	1 µL
ATP (10 mM)	2 µL
DTT (10 mM)	1 µL
T4 ligase (400 000 U/ µL)	0,5 µL
BbsI-HF (20 000 units/ µL)	1 µL

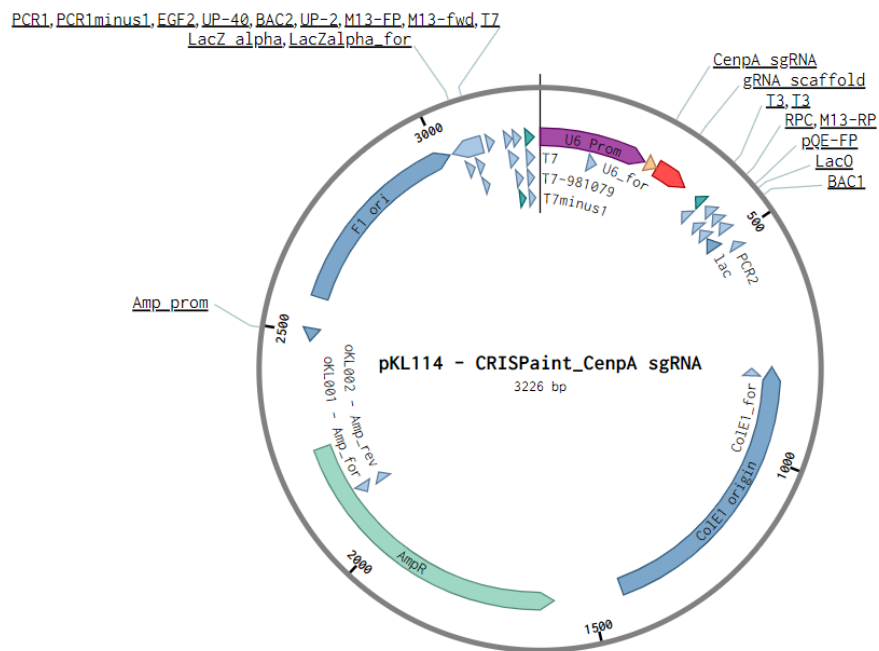
Mixture for Golden Gate assembly was incubated on a thermal cycler at 37 °C for 5 min and then at 21 °C for 5 min interchangeably for 6 consecutive cycles, following ligation at room temperature for 1 h.

Plasmids constructed from pKL114-CRISPaint plasmid: PRC1, Astrin and CenpA are shown in **Figure 10.** and **Figure 11.**





A



B

**Figure 11.** (A) Constructed pKL114-CRISPaint-Astrin and (B) pKL114-CRISPaint-CenpA plasmids.

### 3.2.2. Bacterial transformation

All work regarding bacteria was performed under sterile conditions: under flame, on disinfected surfaces and using sterile equipment. Chemically competent bacteria *E. coli* (Stellar™ Competent Cells, Clontech, CA, USA) were transformed with plasmids obtained from the previous reaction. Transformation was executed using the manufacturer's protocol. After thawing the frozen bacteria, 50 µL of competent bacterial cells were transformed with 3 ng of plasmid DNA. Tubes were placed on ice for 30 min and then heat shocked for 60 sec at 42 °C. After the heat shock, cells were again placed on ice for 2 min. To recover the bacteria, 450 µL of SOC medium (prewarmed at 37 °C) was added to the tube. Cells were then incubated for 1 h at 30 °C on a shaker (250 rpm).

When Stellar™ Competent Cells were not available, *E. coli* C600 were used, but they had to be made competent first. After thawing the cells, a small amount of them was taken using a plastic tip, put in 3 mL of liquid LB medium and incubated at 30 °C on a shaker (250 rpm) overnight. Optical density (OD) was measured the next day and bacteria had to be diluted to 0,1 OD in a 50 mL Falcon tube. Cells were then incubated for around 1 h at 30 °C on a shaker (250 rpm) or after OD reached the value of 8,0. After that, cells were pelleted by centrifugation for 10 min at 4 000 rpm at 4 °C. 500 µL cold transformation/storage buffer (TSB) was then used to resuspend the pellet gently and tubes were incubated on ice for 1,5 h. To transform the cells, 3 µg of plasmid DNA was added to 50 µL of C600 cells and they were incubated on ice for another 30 min. Then, 250 µL of TSB + 1 mL of 40 % glucose was added and tubes were incubated for 1 h at 30 °C on a shaker (250 rpm).

Transformed bacterial mixture was then plated on LB agar solid plates with 1 mg/mL ampicillin for selection using 100 µL of cells for each plate. Bacteria were incubated at 37 °C overnight. Individual colonies were then picked using a plastic tip and put into liquid LB medium with 1 mg/mL ampicillin. Tubes were incubated for 9 h at 30 °C on a shaker (250 rpm).

### 3.2.3. Plasmid isolation

Plasmids cloned in overnight cultures were isolated using QIAprep Spin Miniprep Kit. The isolation was executed using the manufacturers' protocol. Bacterial overnight culture was added to a microcentrifuge tube and pelleted by centrifugation in for 3 min at 8 000 rpm at room temperature. After resuspending bacterial cells in a buffer, lysis buffer was added and the tube

was inverted 4-6 times. The solution was next neutralized using a neutralizing buffer and cells were centrifuged for 10 min at 13 000 rpm. The supernatant was then applied to spin columns and centrifuged for 1 min at 13 000 rpm. After washing the column, plasmid DNA was eluted using the elution buffer.

The concentration of eluted plasmid DNA was measured on Qubit 4 Fluorometer (Thermo Fisher Scientific Inc., Waltham, MA, USA).

To obtain plasmid concentrations sufficient for transfection, plasmid DNA was again cloned in overnight cultures following previously mentioned protocol and isolated using NucleoBond Xtra Midi Plus EF kit.

### 3.2.4. Restriction digestion

Restriction enzyme digestion was performed on constructed plasmids after both, Golden Gate assembly and Mini prep to check if they were properly cut and ligated with sgRNA sequence. Two restriction enzymes were used in the reaction. BbsI-HF cut the plasmid in the previous Golden Gate assembly reaction and because of loss of that restriction place, this enzyme does not cut a successfully constructed plasmid. Second restriction enzyme that was used was BsaI-HF that makes a cut in a place further from BbsI-HF restriction place. Empty plasmid pKL114 was used as negative control. Reaction conditions are shown in **Table 3**.

**Table 3.** The reaction mixture for restriction digestion, for a single sample.

Reactants	Quantity
Cutsmart buffer (10X)	1 $\mu$ L
BbsI-HF (20,000 units/mL)	0,1 $\mu$ L
BsaI-HF (20,000 units/mL)	0,1 $\mu$ L
plasmid	150 ng
nuclease free water	until final volume reaches 10 $\mu$ L

Samples were incubated in a thermoblock at 37 °C for 2 h.

Agarose gel-electrophoresis was carried out on a 1,25 % with addition of SYBR Safe gel stain. Gel-electrophoresis was run gel in 1x TAE Buffer (Tris-acetate-EDTA) at 70 V for 40 min. Gels were imaged on Uvidoc HD6 (Uvitec, Cambridge, England, UK).

### **3.2.5. Plasmid DNA sequencing**

To ensure that the whole sequence for sgRNA was inserted in the plasmid as well as in the right orientation, plasmids had to be sequenced. Samples were prepared by mixing 5  $\mu$ L of purified plasmid (100 ng/ $\mu$ L) and 5  $\mu$ L of sequencing primer U6 (10 pmol/ $\mu$ L). After labeling, samples were sent to Macrogen Europe (Amsterdam, Netherlands) where Sanger sequencing was performed.

U6 forward universal primer: 5' – TAGAAAGTAATAATTTCTTGGG – 3'

### **3.2.6. Cell culture**

For the purposes of this experiment, two different cell lines were used. RPE1 cell line made puromycin sensitive (RPE1 PuroS) and HeLa cell line stably expressing mCherry-CenpA. Cells were cultured in a 75 cm<sup>2</sup> sterile flask in Dulbecco's Modified Eagle Medium (1 g/L D-glucose, pyruvate and L-glutamine, DMEM, Capricorn Scientific GmbH, Ebsdorfergrund, Germany) with 10% (vol/vol) heat-inactivated Fetal Bovine Serum (FBS; Sigma-Aldrich, St. Louis, Missouri, US) and 10000 U/mL penicillin/streptomycin solution (Lonza, Basel, Switzerland). Cells were kept at 37 °C and 5 % CO<sub>2</sub> in a Galaxy 170 R CO<sub>2</sub> humidified incubator (Eppendorf, Hamburg, Germany).

Cells were passaged approximately every 48-72 hours or when they reached around 70-80% confluency. Old medium was aspirated and flask was washed with 10 mL of Phosphate-Buffered Saline (PBS). Cells were then incubated in 1 mL 1% trypsin/EDTA (Biochrom AG, Berlin, Germany) for 5 minutes at 37 °C and 5 % CO<sub>2</sub>. After incubation, approximately 5 mL of DMEM pre-warmed at 37 °C was added to the cells to inactivate trypsin. Between 0,5 and 1 mL of cell suspension was left the flask and 10 mL of pre-warmed DMEM was added for further growth.

### **3.2.7. Transfection using FuGENE HD transfection agent**

For plasmid transfection, cells were grown in a 100 mm diameter plate (TC-treated Culture Dishes, Corning, NY, USA) until reaching ~50% cell confluency. To achieve this confluency, 240 000 RPE1 PuroS and 600 000 HeLa mCherry-CenpA cells were plated in 10 mL of DMEM.

Cells were transfected the next day with three plasmids simultaneously by chemical transfection using FuGENE HD Transfection Reagent (Promega Corporation, Madison, WI USA). Desired concentration of plasmid DNA for each was 2,5  $\mu\text{g}/\mu\text{L}$  for all plasmids. Frame plasmids used in transfection were pCas9-mCherry-Frame+1 for TUBB and CenPA targeting plasmids and pCas9-mCherry-Frame+2 for Astrin and PRC1 targeting plasmids (**Figure 12.**), pCRISPaint-TagGFP2-PuroR donor plasmid (**Figure 13.**) pCas9-mCherry-TubB targeting plasmid (**Figure 14.**) and constructed targeting plasmids pKL114-CRISPaint-PRC1, pKL114-CRISPaint-Astrin and pKL114-CRISPaint-CenpA. Reading frame corrections for these proteins and their corresponding sgRNAs were chosen with the help of Benchling platform.

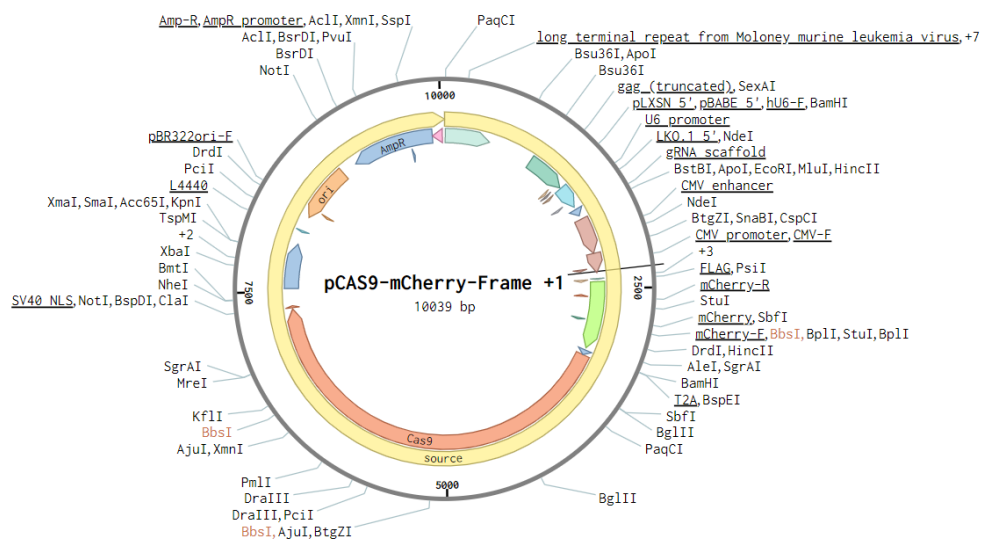
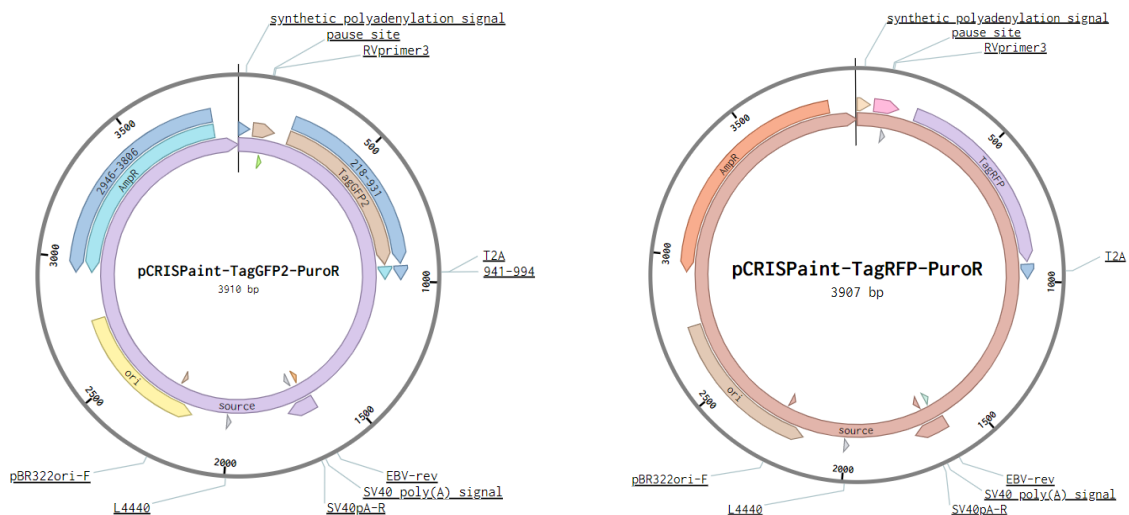


**Figure 12.** Map of the pCas9-mCherry-Frame+1 plasmid; pCas9-mCherry-Frame0/+2 maps are the same, the difference is one nucleotide for the compensation of shifted frame.





aspirated and fresh medium was added to the cells. After 48 h the medium was exchanged for fresh medium with 3  $\mu\text{L}$  of supplemental antibiotic puromycin.

### 3.2.8. Electroporation

As an alternative to FuGENE mediated transfection, RPE1 PuroS and HeLa cell lines were also transfected by electroporation using Amaxa Cell Line Nucleofector Kit R in Nucleofector 2b device (Lonza, Basel, Switzerland). To pre-warm the medium for electroporated cells, DMEM was previously put into 75  $\text{cm}^2$  flasks and left in the incubator. Two mixtures prepared are shown in **Table 5**.

**Table 5.** Reaction mixtures of electroporation.

Reactants	Quantity	Reactant	Quantity
pCas9-mCherry-Frame+1	5 $\mu\text{g}$	Nucleofector solution R	110 $\mu\text{L}$
pCRISPaint-TagGFP2-PuroR	5 $\mu\text{g}$		
Target selector plasmid	5 $\mu\text{g}$		
Final volume	40 $\mu\text{L}$		

Cells were trypsinized, collected and  $1 \times 10^6$  cells were counted and put into a tube. Cells were then centrifuged and supernatant was completely removed. Cells were resuspended in the Nucleofector solution R and the whole suspension was added in the plasmid mixture tube. Suspension was put into a cuvette and then in the electroporation machine (Lonza, Basel, Switzerland). Around 100  $\mu\text{L}$  of warm DMEM from the flask was added to the cuvette, and after resuspending, the mixture of cells and plasmids was evenly distributed into the flask. Cells were then incubated at 37  $^{\circ}\text{C}$  and 5 %  $\text{CO}_2$ . The next day the medium with the Nucleofector was aspirated and fresh medium was added to the cells. After 48 h the medium was exchanged for fresh medium with 3  $\mu\text{L}$  of antibiotic puromycin. Medium with supplemented antibiotic was replaced every 2-3 days. The target selector plasmids used were pCas9-mCherry-TubB and pKL114-CRISPaint-CenpA.

### 3.2.9. Fixation and staining

For microscopy imaging,  $2 \times 10^5$  of both RPE1 PuroS and HeLa mCherry-CenpA transfected cells was plated and cells were grown on glass bottom dishes (14 mm, No. 1.5H,

ibidi GmbH, Gräfelfing, Munich, Germany). The next day, cells were fixed in a fixation solution (3% PFA + 0,25% GLA) pre-warmed at 37 °C for 10 minutes at room temperature. Solution was washed off with 3 washes in 1x PBS. For permeabilization, fixed cells were incubated in 0,5% Triton in 1x PBS for 15 minutes at RT on the shaker at low speed. Triton was then washed off with 3 washes in 1x PBS, 5 minutes each wash.

To visualize cell membrane, SiR-actin (#SC001, Spirochrome AG, Thurgau, Switzerland) was added to the fixed cells and for chromosome visualization DAPI stain (D9542, Sigma-Aldrich, St. Louis, MO, USA). Solution of 0,2 µL of SiR-actin in 1 mL of DAPI (1 µg/mL in PBS) was added to every dish and cells were incubated for 15 min. The solution was then washed off with 3 washes in 1x PBS, 5 minutes each wash.

### **3.2.10. Immunofluorescence**

For spindle parameters measurements, RPE1 PuroS TUBB-TagGFP2 and HeLa mCherry-CenpA TUBB-TagGFP2 and their control cells were plated. The next day, the medium was removed from the dishes and 500 µL of cytoskeleton extraction buffer (CEB) pre-warmed at 37 °C was added to each sample. Cells were incubated in CEB for 1 min, then fixed and permeabilized. Next, cells were blocked in blocking buffer, 1% normal goat serum (NGS) in 1x PBS for one hour at 4 °C on the shaker on low speed. Blocking buffer was washed off with three washes of PBS, 5 minutes each wash. Primary rat monoclonal anti- $\alpha$ -tubulin antibody (MA1-80017, Thermo Fisher Scientific Inc., Waltham, USA) was prepared in blocking buffer as 1:300 dilution, 300 µL for each 3.5 cm dish. Primary antibody was added into the dish and put into a Petri dish. To prevent drying of antibody solution, Petri dish was inlaid with a wet paper towel inside, covered and sealed with parafilm. Cells were incubated overnight at 4 °C. Primary antibody was washed three times with 1x PBS at RT while shaking gently on a shaker, 5 minutes each wash. Secondary donkey anti-rat AlexaFluor 594-conjugated antibody (#ab150156, Abcam, Cambridge, UK) was diluted in 2% NGS in 1x PBS to 1:1000 and 250 µL of diluted secondary antibody was added on the cells. The dish was covered with aluminum foil and incubated on the shaker for one hour at room temperature. Secondary antibody was then washed off with 3 washes in 1x PBS while shaking gently, 5 minutes each wash. Finally, to visualize chromosomes, cells were incubated in SiR-DNA (#SC007, Spirochrome AG, Thurgau, Switzerland), 1 µL in 1 mL PBS solution, for 30 min at room temperature. SiR-DNA

was then washed off with 2 washes in 1x PBS while shaking gently, 5 minutes each wash. Until microscopy imaging, samples were stored at 4 °C.

### **3.2.11. Confocal microscopy imaging**

Confocal Z-series stacks and tile regions with multiple positions of fixed, SiR-actin and DAPI stained cells was performed on Zeiss LSM800 confocal laser scanning microscope with Airyscan (Carl Zeiss AG, Jena, Germany). Imaging was performed using the 63x/1,4NA DIC Plan-Apochromat oil immersion objective (Carl Zeiss AG, Jena, Germany). The system was controlled with the ZEN 3.5 software (Carl Zeiss AG, Jena, Germany). The 405 nm, 488 nm and 605 nm laser lines were used to excite DAPI, TUBB-TagGFP and SiR-actin, respectively. The laser intensities were 1,0 % for the 45 nm line, 4,5 % for the 488 line and 3,0 % for the 605 nm line. Images were made using "Tiles" function which allows capturing of multiple fields in proximity that are at the end arranged into a grid. For every tile, 7 focal planes were acquired with z-step size of 1 µm.

Confocal microscopy of immunostained cells and live-cell imaging were performed using an Expert Line easy3D STED microscope system (Abberior Instruments, Göttingen, Germany) equipped with Olympus IX83 inverted microscope (Olympus, Tokyo, Japan). STED and confocal microscopy of immunostained cells were performed with the 100x/1,4NA UPLSAPO oil immersion objective (Olympus, Tokyo, Japan) and an avalanche photodiode (APD). The system was controlled with the Inspector Software Package for Data Acquisition and Analysis (Abberior Instruments, Göttingen, Germany). The 405 nm and 594 nm laser lines were used to excite SiR-DNA and anti-rat donkey 594 antibody, respectively. The laser intensity was 20 % for 405 nm line and 30 % for 594 line while STED resolution for 594 nm line was at 50 %. The xy pixel size was 30 nm and 10-20 focal planes were acquired with z-step size of 300 nm. Live-cell imaging was performed with the 60x/1,2NA UPLSAPO water immersion objective (Olympus, Tokyo, Japan) and the APD detector. Cells were kept at 37 °C and 5 % CO<sub>2</sub> in OKOLAB stage top heating gas chamber (Okolab, Pouzzoli, Naples, Italy). For optimal signal-to noise ratio, the pinhole diameter was set to 1 AU. To obtain time series images, the xy pixel size was 100 nm and 10-20 focal planes were acquired with z-step size of 1 µm at 60 s time intervals between frames.

### 3.2.12. Image analysis

Microscopy image processing and analysis were performed in ImageJ (National Institutes of Health, Bethesda, Maryland, US). Images were adjusted for brightness and contrast. Fixed and stained cell tiles were counted using the 'Multi-point' tool. Length and width of mitotic spindles in the metaphase were measured on live and immunostained cells. Measurements of length were performed in ImageJ using the "Straight line" tool and marking the distance between two spindle poles (**Figure 15. A**). If both spindle poles were not visible in a single image slice, distance between poles was calculated using the Pythagorean theorem in which one non-hypotenuse represents distance between poles in average intensity Z projection, other is the distance between stacks in which poles are visible and hypotenuse is calculated for length. Width of the spindle was also measured using the "Straight line" tool in ImageJ marking the distance between two furthest microtubules in a spindle (**Figure 15. B**). To incorporate every slice of the image, width measurement was performed on average intensity Z projection.

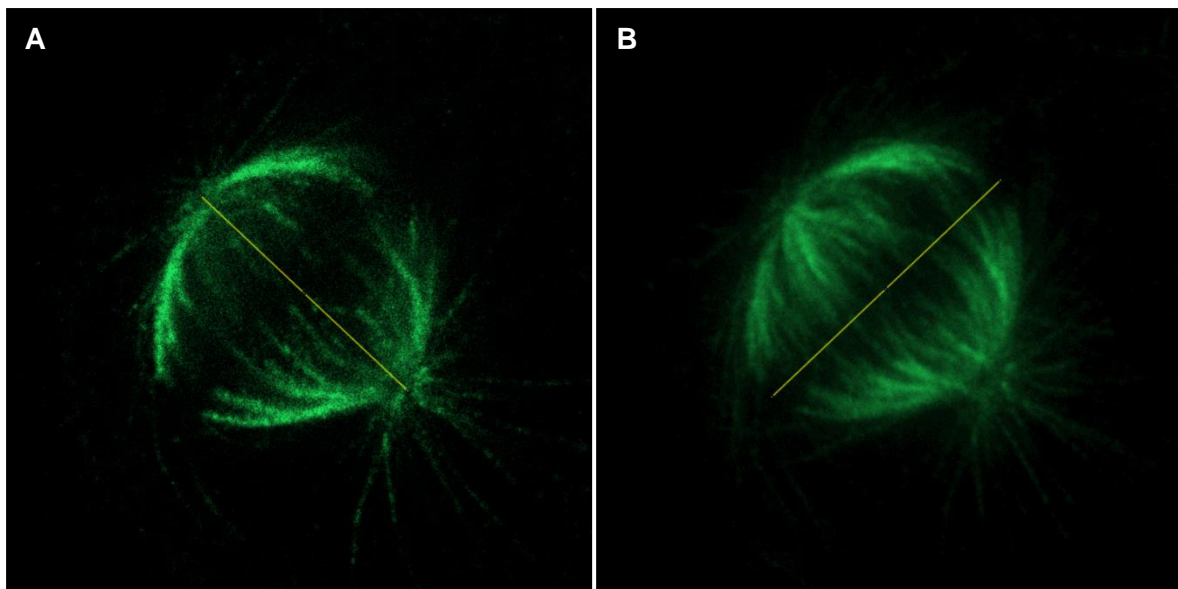


**Figure 15.** Measurement of spindle parameters. (A) Measurement of pole-to-pole spindle length. (B) Measurement of spindle width using Z-projection of average intensities of all stacks. Images obtained using a confocal microscope.

## 4. Results

### 4.1. Establishment of HeLa cell line stably expressing TUBB-TagGFP2

HeLa mCherry-CenpA cell line was transfected with pCRISPaint-TagGFP2-PuroR donor plasmid and pCas9-mCherry-TubB target plasmid. Determined frame correction for insertion of the tag in the right reading frame was +1, thus pCas9-mCherry-Frame+1 plasmid was also used. Transfection was executed using FuGENE HD transfection agent. Optimal selection after transfection showed to be addition of puromycin starting with concentration of 2  $\mu\text{g}/\text{mL}$  first and continuing with 3  $\mu\text{g}/\text{mL}$ . Initial concentration of puromycin was slightly lower than the one required for selection to reduce cell stress after transfection and gradually introduce the selection antibiotic. After around one week of selection, cells were checked for signal on a STED confocal microscope. TagGFP2 signal was visible in the cells and live-cell images were acquired (**Figure 16**). EGFP (488 nm) laser line (20 % intensity) was used for TagGFP2 and STAR 580 (580 nm) laser line (10 % intensity) for mCherry-CenpA were used. Time series that cover the progression of mitosis through phases were also acquired (**Figure 17**.) Images were acquired in 60 s intervals to reduce overall laser exposure of the cells. Not every cell expressed TUBB-TagGFP2 and signal intensity varied between some cells. Metaphase to anaphase live-cell imaging has shown that these cells divide normally.

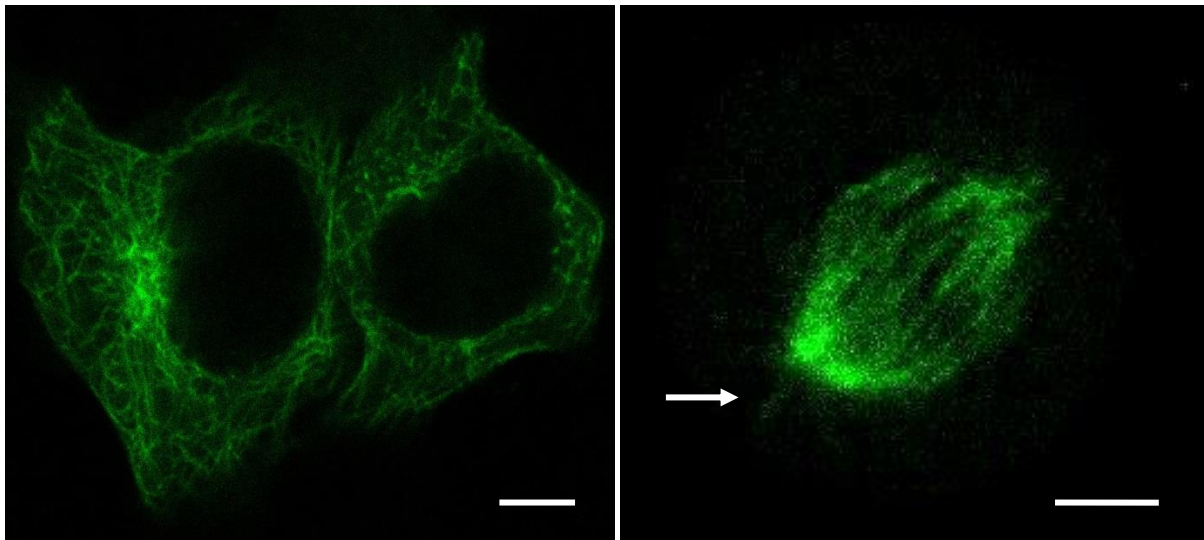


**Figure 16.** (A) Two HeLa mCherry-CenpA TUBB-TagGFP2 cells in the interphase. Microtubule network is visible in green as a result of successful TagGFP2 tag integration and expression of TUBB-TagGFP2 fusion protein. (B) HeLa mCherry-CenpA TUBB-TagGFP2

mitotic spindle, arrow shows slightly visible astral microtubule. Image obtained using STED confocal microscope. Scale bar 5  $\mu\text{m}$ .

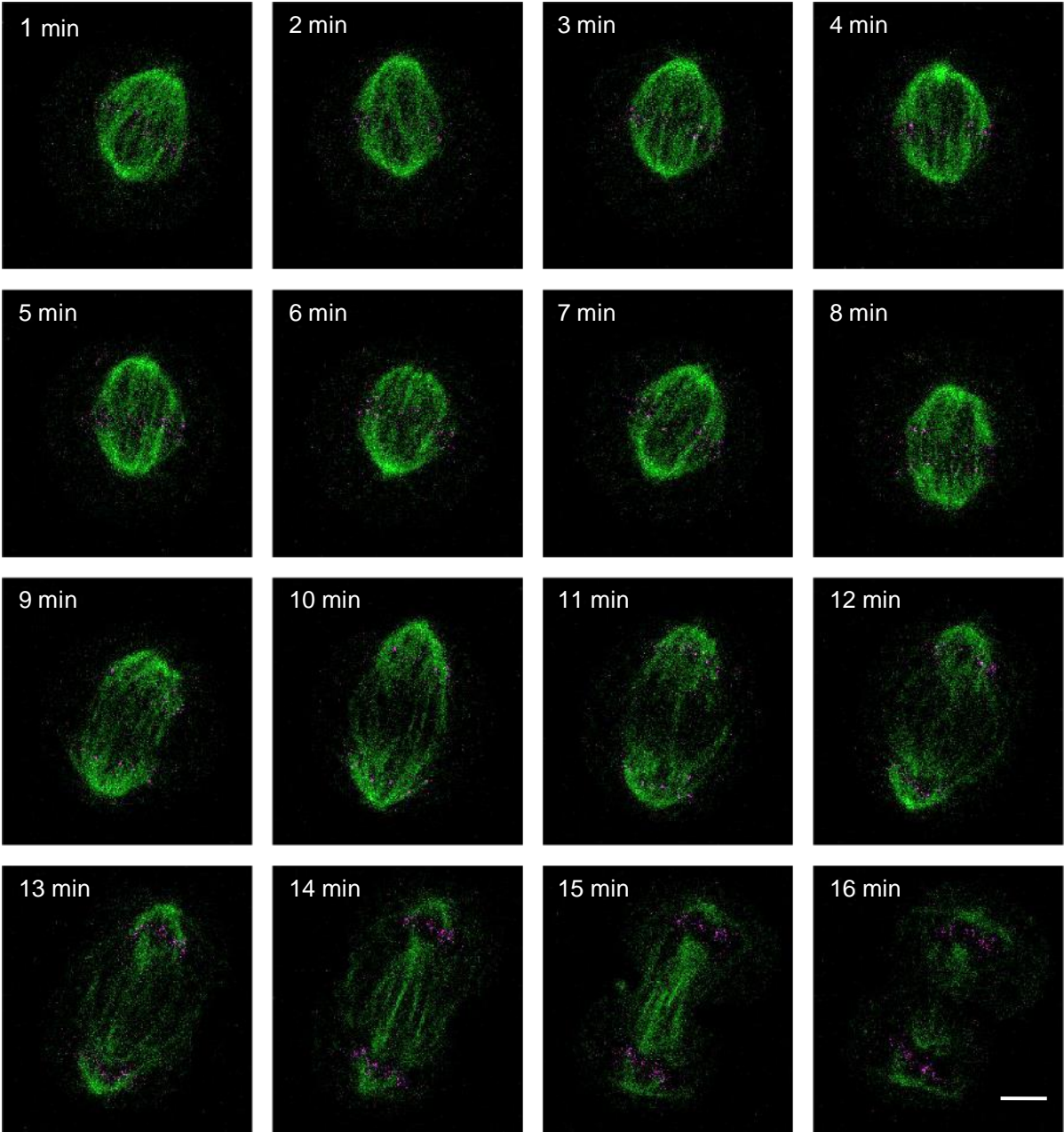


**Figure 17.** HeLa mCherry-CenpA TUBB-TagGFP2 cell division from metaphase to telophase. TUBB-TagGFP2 is shown in green and mCherry-CenpA in magenta. Image obtained using STED confocal microscope. Scale bar 5  $\mu\text{m}$ .

## 4.2. Establishment of RPE1 cell line stably expressing TUBB-TagGFP2

RPE1 PuroS cells were transfected under the same conditions as previously described for HeLa mCherry-CenpA TUBB-TagGFP2 cells. Expansion of transfected RPE1 PuroS cells lasted for approximately one month before acquiring live-cell images, around four times longer than HeLa cells. Confocal imaging showed successful integration of TagGFP2 into the genome and expression TUBB-TagGFP2 fusion protein in RPE1 PuroS cells (**Figure 18.**). EGFP (488 nm) laser line (20 % intensity) was used for TagGFP2. As in HeLa mCherry-CenpA TUBB-TagGFP2, these cells also showed slightly varied signal presence and intensity. Time series that show the progression of mitosis through phases were also acquired and are shown in **Figure 19.** Metaphase to anaphase live-cell imaging has shown that these cells divide normally. Images were acquired with EGFP laser at 15 % in 60 s intervals to reduce overall laser exposure of the cells.

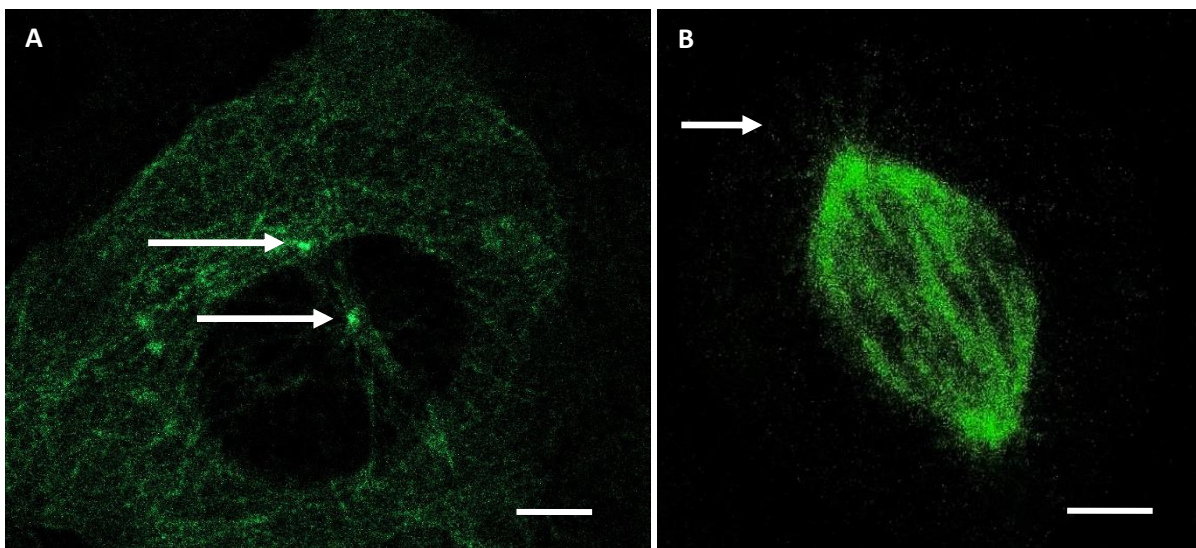


**Figure 18.** (A) RPE1 PuroS TUBB-TagGFP2 cell in the interphase. Arrows show two microtubule organizing centers (centrosomes). (B) RPE1 PuroS TUBB-TagGFP2 mitotic spindle, arrow shows slightly visible astral microtubules. Image obtained with STED confocal microscope. Scale bar 5  $\mu\text{m}$ .

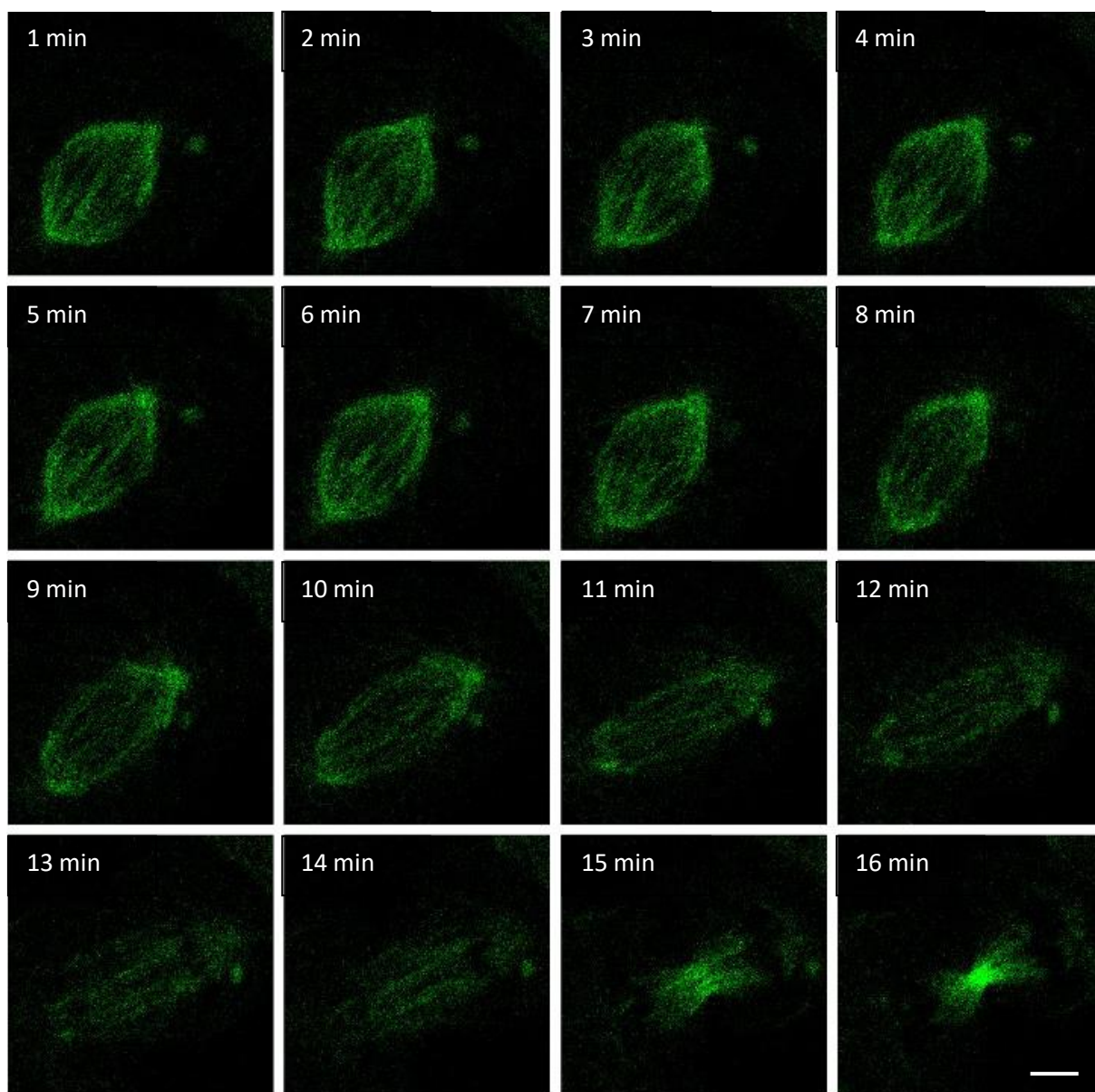


**Figure 19.** RPE1 PuroS TUBB-TagGFP2 cell division from metaphase to telophase. Image obtained using STED confocal microscope. Scale bar 5  $\mu$ m.

### 4.3. Transfection efficiency

To evaluate transfection efficiency, large fields of cells were captured using Zeiss LSM800 microscope with the function 'Tiles'. Cells were counted to determine the percentage of cells stably expressing TUBB-TagGFP2. **Figure 20.** shows HeLa mCherry-CenpA TUBB-TagGFP2 cells fixed and stained with DAPI and SiR-Actin. Virtually every cell had signal and most of them showed signal in the nucleus as well as in the cytoplasm. Signal intensity varied.

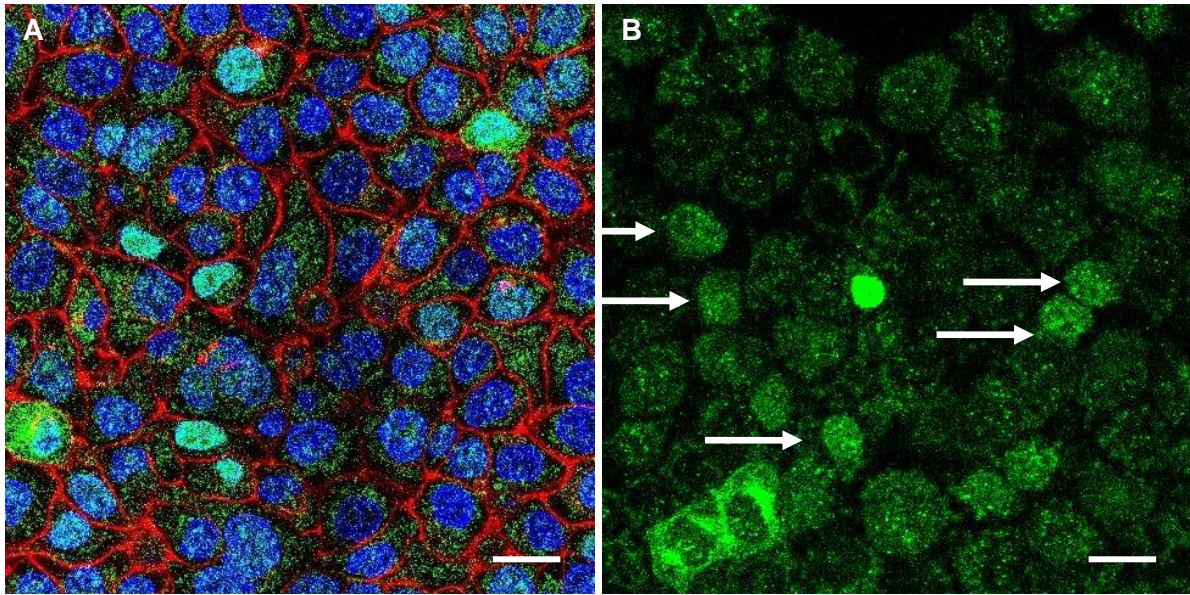


**Figure 20.** HeLa mCherry-CenpA TUBB-TagGFP2 fixed and stained cells. (A) Green: TUBB-TagGFP2, blue: DNA (DAPI), red: actin (SiR-actin). (B) Green: TUBB-TagGFP2, strong signal can be seen in the nucleus of some cells (arrows). Image obtained using Zeiss LSM800 confocal microscope. Scale bar 10  $\mu\text{m}$ .

Counting of RPE1 PuroS TUBB-TagGFP2 cells revealed that 97.3 % contained TUBB-TagGFP2 (**Figure 21.**), no cells were found to have signal in the nucleus.

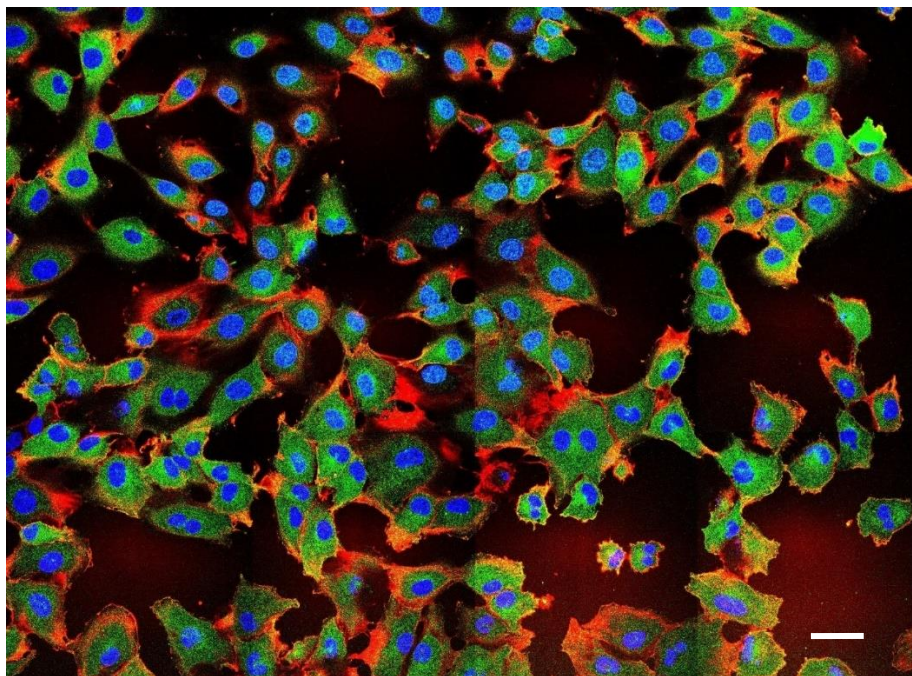


**Figure 21.** HeLa mCherry-CenpA TUBB-TagGFP2 fixed and stained cells. (A) Green: TUBB-TagGFP2, blue: DNA (DAPI), red: actin (SiR-actin). Image obtained using Zeiss LSM800 confocal microscope. Scale bar 10  $\mu\text{m}$ .

#### 4.4. Immunofluorescence images

To evaluate spindle morphology of transfected cells, they were fixed and immunostained for tubulin. This step was required to see the morphology of the spindle in more detail and precisely measure its parameters. In order to find and image cells in metaphase, SiR-DNA was added to immunostained cells to visualize the chromosomes. Cells that were found in metaphase were checked for TagGFP2 signal before acquiring the image to ensure capturing of successfully transfected cells only. One such mitotic spindle of HeLa mCherry-CenpA tub-GFP2 recorded after TagGFP2 excitation using the EGFP laser setting (488 nm line) at 30% intensity is shown in **Figure 22**.

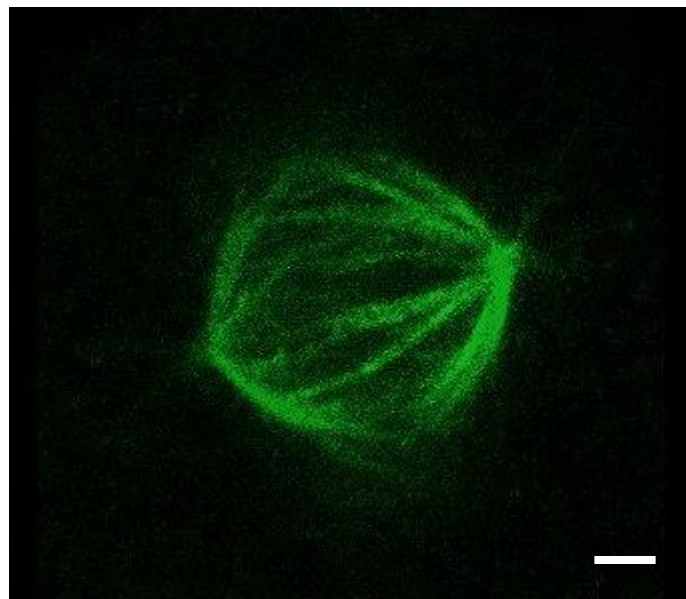


**Figure 22.** Maximum intensity Z-projections of HeLa mCherry-CenpA TUBB-GFP2 mitotic spindle in metaphase. TagGFP2 is depicted in green. Immunocytochemically fixed, imaged on STED microscope. Scale bar 2  $\mu\text{m}$ .

Cells that were in metaphase and possessed TagGFP2 signal were imaged. Example of an image of a cell in metaphase acquired on a confocal microscope is shown in **Figure 23**. Spots of SiR-DNA dye can be visible outside of the spindle area. **Figure 24**. shows the spindle of a RPE1 PuroS TUBB-TagGFP2 cell immunostained for tubulin in STED resolution.

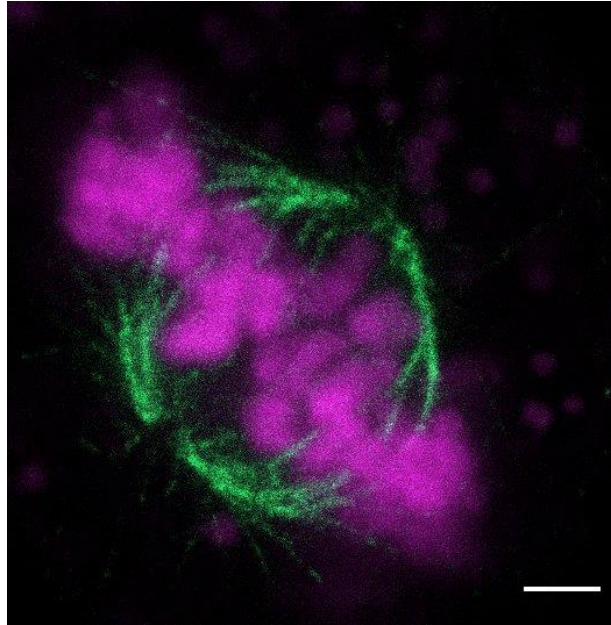


**Figure 23.** HeLa mCherry-CenpA TUBB-GFP2, green:  $\alpha$ -tubulin (anti- $\alpha$ -tubulin594), magenta: chromosomes (sirDNA, 1 $\mu$ M). Immunocytochemically fixed and imaged on STED microscope, scale bar 2  $\mu$ m.

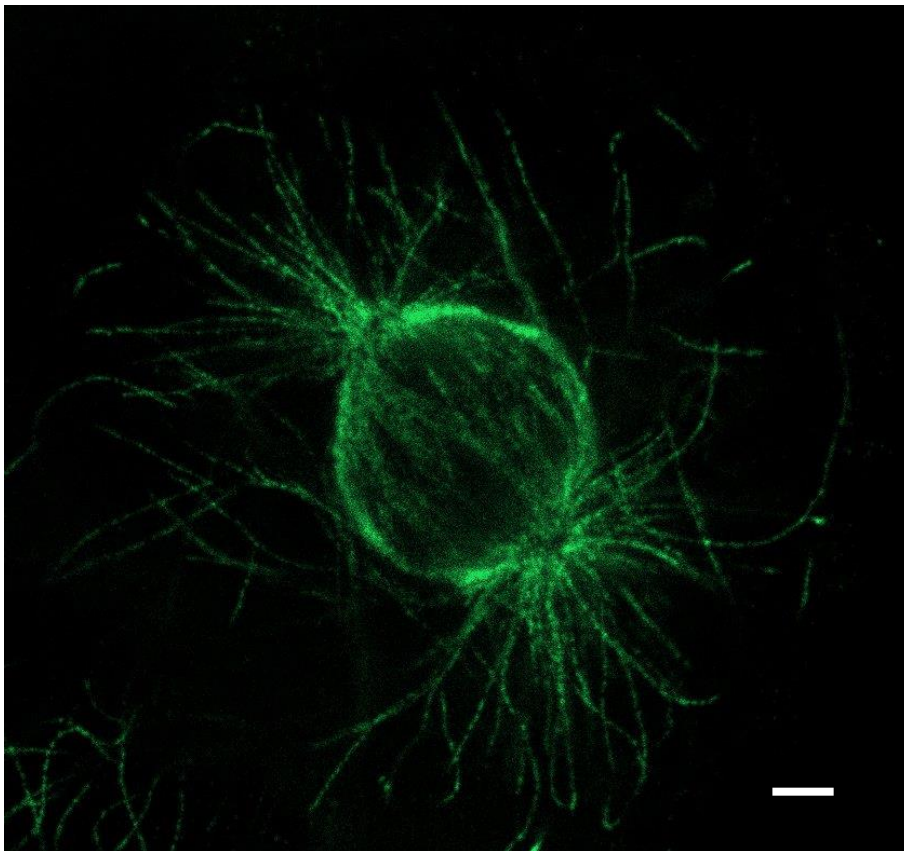


**Figure 24.** RPE1 PuroS TUBB-TagGFP2, green:  $\alpha$ -tubulin (anti- $\alpha$ -tubulin594) in STED resolution. Immunocytochemically fixed and imaged on STED microscope, scale bar 2  $\mu$ m.

## 4.5. Spindle length and width measurements

Metaphase spindle length of RPE1 PuroS TUBB-TagGFP2 and HeLa mCherry-CenpA TUBB-TagGFP2 cells were measured in ImageJ and statistically analyzed. Non-transfected controls were also measured for mitotic spindle length to evaluate newly obtained cell lines.

Average lengths of spindles are shown in **Figure 25**, including standard deviation error bars. The results suggest that spindles of transfected cells tend to be slightly shorter. Average spindle length of RPE1 TUBB-TagGFP2 cells is 7,957  $\mu\text{m}$  while their control cells have an average length of 8,615  $\mu\text{m}$ . As for HeLa mCherry-CenpA, length of the control cells is 10,573  $\mu\text{m}$ , while average length of HeLa mCherry-CenpA TUBB-TagGFP2 is 8,463  $\mu\text{m}$ .

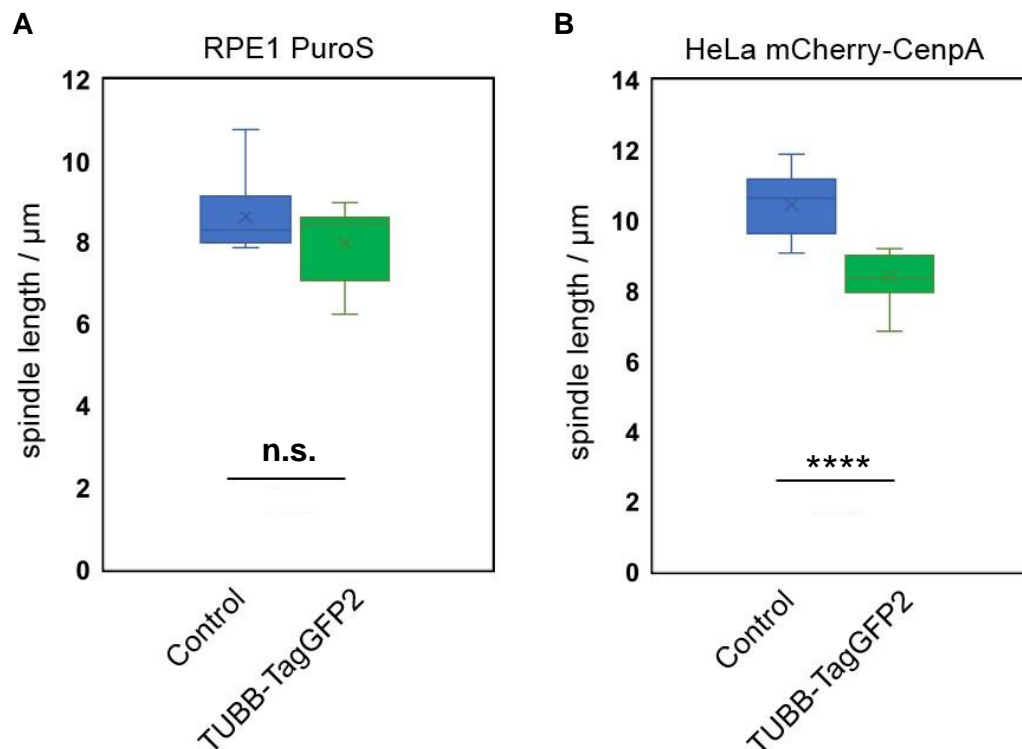


**Figure 25.** Spindle length measurement results. (A) Spindle length of control and TUBB-TagGFP2 expressing RPE1 PuroS cells;  $p=0,263$ ;  $N=11$ . (B) Spindle length of control and TUBB-TagGFP2 expressing HeLa mCherry-CenpA cells;  $p<0,00001$ ;  $N=12$ . Statistical analysis: Mann-Whitney U test, p-value legend:  $<0,0001$  (\*\*\*\*),  $0,0001-0,001$  (\*\*\*),  $0,001-0,01$  (\*\*),  $0,01-0,05$  (\*),  $\geq 0,05$  (not significant=n.s.)

Average widths of spindles are shown in **Figure 26.** with standard error bars. These results show even smaller difference in spindle morphology between control and transfected cells. Average spindle width of RPE1 PuroS TUBB-TagGFP2 cells is 7,569  $\mu\text{m}$  while their control cells have an average width of 8,283  $\mu\text{m}$ . As for HeLa mCherry-CenpA, width of the control cells is 8,761  $\mu\text{m}$ , while average width of HeLa mCherry-CenpA TUBB-TagGFP2 is 8,635  $\mu\text{m}$ .

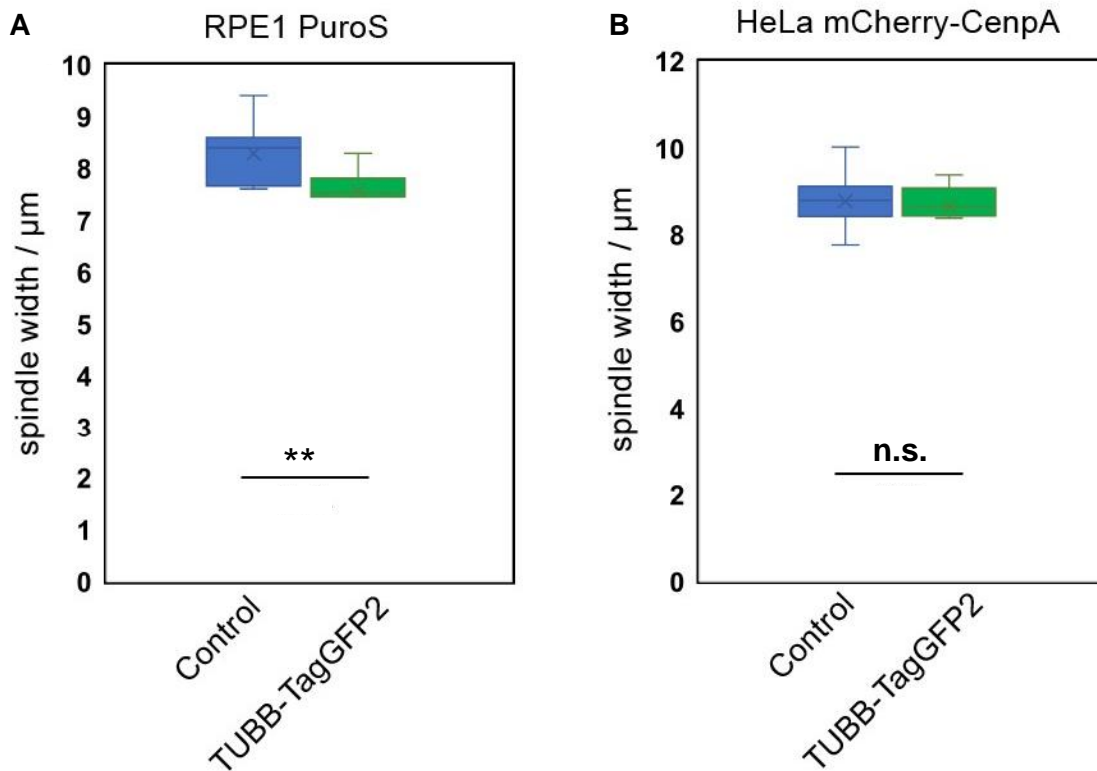


**Figure 26.** Spindle width measurement results. (A) Spindle width of control and TUBB-TagGFP2 expressing RPE1 PuroS cells;  $p=0.0388$ ;  $N=11$ . (B) Spindle width of control and TUBB-TagGFP2 expressing HeLa mCherry-CenpA cells;  $p=0.888$ ;  $N=12$ . Statistical analysis: (A) two-tailed t-test, (B) Mann–Whitney U test, p-value legend :  $< 0.0001$  (\*\*\*\*),  $0.0001–0.001$  (\*\*\*),  $0.001–0.01$  (\*\*),  $0.01–0.05$  (\*),  $\geq 0.05$  (n.s.).

Lengths of live and fixed and immunostained cells were also separately compared (**Figure 27.**). Live cells were measured in the same way as immunostained cells and for the lengths of immunostained cells, previously shown data was used.

Both cell lines showed shrinkage of the mitotic spindles when fixed in comparison to live images. Rpe1 PuroS TUBB-TagGFP2 averaged to 12,019  $\mu\text{m}$  when imaged live and 7,957  $\mu\text{m}$

after immunostaining while HeLa mCherry-CenpA TUBB-TagGFP2 averaged to 11,553  $\mu\text{m}$  when imaged live and 8,462  $\mu\text{m}$  after immunostaining.

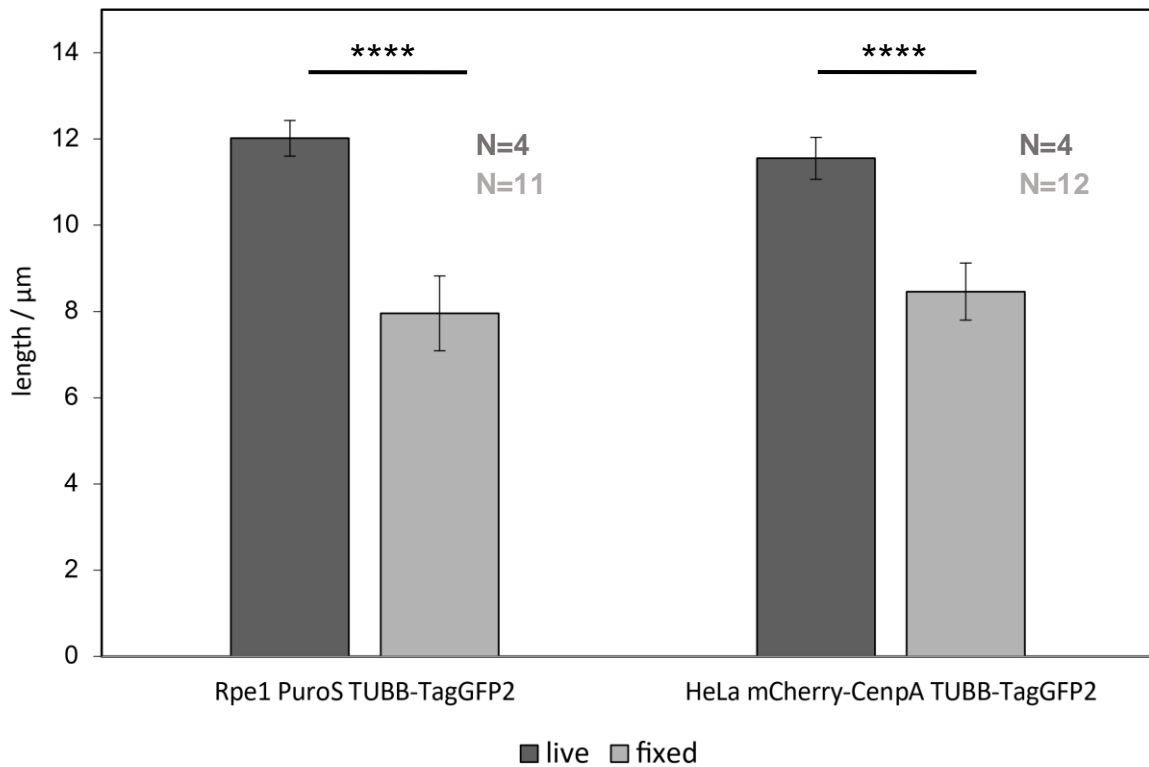


**Figure 27.** Length difference between live and immunostained RPE1 PuroS TagGFP2 and HeLa mCherry-CenpA TUBB-TagGFP2 cells. Statistical analysis: two-tailed t-test, p-value legend: <0,0001 (\*\*\*\*), 0,0001–0,001 (\*\*\*) , 0,001–0,01 (\*\*), 0,01–0,05 (\*),  $\geq 0,05$  (n.s.).

#### 4.6. Transfection trials results

Cell lines HeLa and RPE1 were also transfected with constructed target selector plasmids pKL114-CRISPaint-PRC1, pKL114-CRISPaint-Astrin and pKL114-CRISPaint-CenpA and both universal donor plasmids: pCRISPaint-TagGFP2-PuroR and pCRISPaint-TagRFP-PuroR. **Table 6.** shows combinations of plasmids and outcomes of transfection performed using FuGENE HD transfection agent and **Table 7.** shows combinations of plasmids and outcomes of transfection performed using electroporation with Nucleofector solution R in the Nucleofector 2b device.

As **Table 6.** shows two cell lines were established: RPE1 PuroS TUBB-TagGFP2 and HeLa mCherry-CenpA TUBB-TagGFP2. For RPE1 PuroS, other target-protein combinations resulted in dead cells after selection. As for HeLa cells only PRC1-TagGFP2 and SPAG5-TagGFP2 combinations left viable cells after selection, but signal was not present.

**Table 6.** Outcomes of transfection of two cell lines with combinations of target selector and donor plasmids. Transfection was performed using FuGENE HD transfection agent. Character description: successful transfection (+), no signal present (-), dead cells (x).

Cell line	Target protein-tag					
	TUBB-TagGFP2	CenpA-TagGFP2	CenpA-RFP	TUBB-RFP	PRC1-TagGFP2	SPAG5-TagGFP2
RPE1	+	x	x	x	x	x
HeLa	+	x	x	x	-	-

**Table 7.** Outcomes of transfection of two cell lines with combinations of target selector and donor plasmids. Transfection was performed using electroporation with Lonza machine and Nucleofector. Character description: successful transfection (+), no signal present (-), dead cells (x), unspecific signal (0).

Cell line	Target protein-tag	
	TUBB-TagGFP2	CenpA-TagGFP2
RPE1	-	0
HeLa	+	-

Electroporation was performed to try for the same combinations via different transfection method. HeLa mCherry-CenpA TUBB-TagGFP2 was only successfully transfected line. RPE1 PuroS cell line transfected with CenpA-TagGFP2 combination was expanded for three weeks and exhibited signal (**Figure 28.**), but in cytoplasm, instead of in the nucleus.

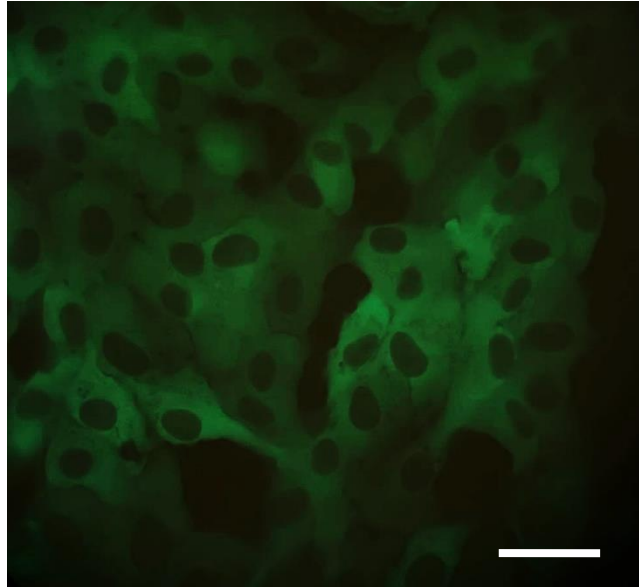


**Figure 28.** RPE1 PuroS cell line transfected with CenpA-TagGFP2 plasmid combination (electroporation). TagGFP2 signal is visible in the cytoplasm. Imaged live on STED confocal microscope. Scale bar 10  $\mu\text{m}$ .

## 5. Discussion

HeLa cell line is widely used in various fields of research such as effects of substances on cells, gene regulation and also fundamental studies on cellular structure and function. In addition, they are easy to grow and maintain in cell culture (Svalastog & Martinelli, 2013). For that reason, it is simpler to establish transfection conditions on them and that is why I used them in my experiment. However, HeLa cells are near-tetraploid and genetically unstable, which can make them an unreliable cell line for studying processes such as mitosis (Scott et al., 2020). This is why, in this experiment, I also used human retinal pigment epithelial (RPE1) cell line that is near-diploid and has a stable karyotype (Hindul et al., 2022). Due to the trait of normal cell lines having limited number of cell divisions, they eventually reach senescence and stop dividing. To maintain their ability to divide, RPE1 cells were immortalized by the human telomerase reverse transcriptase subunit (hTERT) (Bodnar et al., 1998). In the process of immortalization, RPE1 cells were also made puromycin-resistant, but for the purpose of this experiment, I needed puromycin-sensitive cells to execute the selection of successfully transfected cells. For that reason I chose RPE1 cells with puro-resistant gene knocked out (Lambrus et al., 2016).

Here, I explored a novel method of precise insertion of genetic material into genomes developed by Schmid-Burgk et al. (2016) called *CRISPaint*. This is a modular system that utilizes CRISPR-Cas9 to make a site-specific insertion of a tag gene at a C-terminal end of a desired protein in the genome using three different plasmids. For the purpose of this experiment I found four target proteins involved in the mitosis that have all been previously C-terminally tagged, thus were candidates for *CRISPaint* tagging:  $\beta$ -tubulin (Parker et al., 2018), CenpA (Smoak et al., 2016), Astrin (Papini et al., 2021) and PRC1 (Polak et al., 2017).

Using *CRISPaint* I have established two cell lines that endogenously express TagGFP2 tagged  $\beta$ -tubulin: HeLa mCherry-CenpA TUBB-TagGFP2 and RPE1 PuroS TUBB-TagGFP2. Both cell lines were transfected using FuGENE HD, a nonliposomal transfection reagent (Wiesenhofer & Humpel, 2000) that is simple to use and delivers a high percentage of transfection in HeLa cells (Jacobsen et al., 2004). Usage of puromycin resistance cassette enabled selection and enrichment of transfected cells. Expansion of RPE1 cells took around one month, which is four times longer than for HeLa cells which showed expression after one week. This feature of HeLa cells is in line with observations made by Schmid-Burgk et al. (2016). Both cell lines showed sustained fluorescence through passaging with distinguishable

microtubule structures, such as microtubule organizing center, inner spindle and even astral microtubules. Additional expansion period showed high percentage of stably transfected cells for both cell lines, although signal slightly varied between them. Implementation of further selection could provide a homogenous cell line and that is why it would be advisable to perform single-cell cloning. This method is based on diluting the population that contains stably transfected cells as well as untransfected to screen only for those with successful expression. That would allow for acquiring a cell line which has close to 100% effective expression of the protein of interest (Longo et al., 2014). An alternative would be to sort cells on a fluorescence-activated cell sorter (FACS), which is a technique used to separate cells based on having or not having a fluorescence signal (Picot et al., 2012). FACS would also provide a homogenous cell line, but in much shorter time.

I also observed that HeLa mCherry-CenpA TUBB-TagGFP2 cells contained TUBB-TagGFP2 signal in almost all nuclei of interphase cells, which was not expected as tubulin forms a microtubule network in the cytoplasm of the interphase cells. This could be attributed to the localization of  $\beta$ II-tubulin, an isotype of  $\beta$ -tubulin that occurs in nuclei of HeLa and other cancer cell lines. This isotype of tubulin does not build microtubules, but rather complexes with  $\alpha$ -tubulin in a non-microtubule form (Walss-Bass et al., 2002). The sequence of  $\beta$ II-tubulin has a 94,6 % sequence identity to  $\beta$ I-tubulin (TUBB gene) that I targeted via sgRNA. Moreover, 20 amino acids of the C-terminal are completely identical between  $\beta$ I-tubulin and  $\beta$ II-tubulin, which means that sgRNA might be targeting both isotypes (Ludueña, 2013). In contrast, RPE1 PuroS TUBB-TagGFP2 cells show  $\beta$ -tubulin presence only in the cytoplasm, which is consistent with the work of Walss-Bass et al. (2002) that suggests that normal cell lines do not exhibit  $\beta$ II-tubulin localization in the nucleus.

Cells of both established cell lines were imaged in live from metaphase to late anaphase/telophase to observe the cell division in time. Time series showed that both cell lines divide normally and in expected time duration (Chakraborty et al., 2008; Vanpoperinghe et al., 2021).

For evaluating spindle morphology of established cell lines, I performed fixation and immunostaining of the cells including their non-tag-expressing controls. Tubulin was labelled with anti- $\alpha$ -tubulin antibody to visualize the spindle in both non-transfected and transfected cells. I acquired images of the cells in metaphase and measured the length and the width of the spindle. Average length of RPE1 PuroS TUBB-TagGFP2 was 7,567  $\mu$ m while their control cells had an average length of 8,615  $\mu$ m. This result did not show significant difference between

control and transfected cells. However, differences in HeLa spindle length showed to be very significant with spindle length of 8,463  $\mu\text{m}$  of TUBB-TagGFP2 cells and 10,573  $\mu\text{m}$  for control cells. As for width measurements, RPE1 cells showed only slightly significant difference with the width of control cells of 8,283  $\mu\text{m}$  and of TUBB-TagGFP2 cells 7,569  $\mu\text{m}$ . HeLa cells did not exhibit any significant difference in width between control and stably transfected cells.

Spindle shrinkage was also measured for both cell lines upon fixation which has previously observed for HeLa cells (Novak et al., 2018). Lengths of Rpe1 PuroS TUBB-TagGFP2 spindles averaged to 12,019  $\mu\text{m}$  when imaged live and 7,957  $\mu\text{m}$  after immunostaining while HeLa mCherry-CenpA TUBB-TagGFP2 spindle lengths averaged to 11,553  $\mu\text{m}$  when imaged live and 8,462  $\mu\text{m}$  after immunostaining. Lengths for both RPE1 and HeLa in live imaging are consistent with previously described measurements (Štimac et al., 2022).

For the trials, only interesting result is unexpected localization of CenpA in RPE1 PuroS cells transfected with TagGFP2 targeting CenpA. Instead of signal in the nucleus, very distinct signal was present in the cytoplasm. That means that the complete TagGFP2 along with puromycin resistant gene might have been inserted somewhere else in the genome because cells were selected in the antibiotic medium.

Next goal of this experiment would be to tag H2B histone to observe chromosome segregation and compensate for DNA dyes that in my experiments sometimes showed spillage in the other parts of the cell. Moreover, one of the objectives would be to optimize the protocol for RFP transfection and targeting other proteins.

This work also demonstrates that tagging using the *CRISPaint* method is equally successful in cells that express fluorescent signal from a previously accomplished stable transfection since HeLa cell line was already stably transfected with mCherry tagged CenpA protein.

To use this system on puromycin resistant cell lines, donor plasmids that have other antibiotic resistance could be cloned either by modifying pre-existing plasmids or constructing completely new ones.

## 6. Conclusion

I have established two cell lines that endogenously express fluorescently tagged protein tubulin: RPE1 PuroS TUBB-TagGFP2 and HeLa mCherry-CenpA TUBB-TagGFP2. Confocal microscopy imaging showed that transfection using the *CRISPaint* method was successful and that I optimized the protocol for tagging  $\beta$ -tubulin with TagGFP2. This proved that both tumor and non-tumor cell lines were capable of transfection and gene manipulation by the *CRISPaint* system. Moreover, almost all of the microtubule structures, including centrosomes and astral microtubules could be distinguished. Tiles images of HeLa mCherry-CenpA TUBB-TagGFP2 cells showed unexpected presence of tubulin in the nuclei which could be  $\beta$ II-tubulin, a  $\beta$ -tubulin isotype present in the nucleus of some cancer cells. Images obtained in time demonstrated normal cell division of both stably transfected lines. Length measurements of the mitotic spindle showed shorter spindles for HeLa cells after transfection and no difference for RPE1 PuroS. As for width, RPE1 PuroS TUBB-TagGFP2 cells were slightly shorter than control and HeLa cells did not differ between control and transfected.

These cell lines can be further used to study live-cell division dynamics under the confocal microscope, especially HeLa cells that already have tagged CenpA protein. The *CRISPaint* method can be applied to tag other cell lines and with different fluorescent tags.

## 7. Literature

- Alberts, B., Johnson, A., Lewis, J., Morgan, D., Raff, M., Roberts, K., & Walter, P. (2017). Molecular biology of the cell. In *Molecular Biology of the Cell*. Garland Science. <https://doi.org/10.1201/9781315735368>
- Arnal, I., & Wade, R. H. (1995). How does taxol stabilize microtubules? *Current Biology*, 5(8), 900–908. [https://doi.org/10.1016/S0960-9822\(95\)00180-1](https://doi.org/10.1016/S0960-9822(95)00180-1)
- Bétermier, M., Bertrand, P., & Lopez, B. S. (2014). Is non-homologous end-joining really an inherently error-prone process? In *PLoS Genetics* (Vol. 10, Issue 1, p. e1004086). Public Library of Science. <https://doi.org/10.1371/journal.pgen.1004086>
- Bodnar, A. G., Ouellette, M., Frolkis, M., Holt, S. E., Chiu, C. P., Morin, G. B., Harley, C. B., Shay, J. W., Lichtsteiner, S., & Wright, W. E. (1998). Extension of life-span by introduction of telomerase into normal human cells. *Science*, 279(5349), 349–352. <https://doi.org/10.1126/science.279.5349.349>
- Borkholder, D. A. (1998). Cell based biosensors using microelectrodes. *PhD Thesis*, 1–253.
- Carroll, D. (2011). Genome engineering with zinc-finger nucleases. *Genetics*, 188(4), 773–782. <https://doi.org/10.1534/genetics.111.131433>
- Chakraborty, P., Wang, Y., Wei, J. H., van Deursen, J., Yu, H., Malureanu, L., Dasso, M., Forbes, D. J., Levy, D. E., Seemann, J., & Fontoura, B. M. A. (2008). Nucleoporin levels regulate cell cycle progression and phase-specific gene expression. *Developmental Cell*, 15(5), 657–667. <https://doi.org/10.1016/j.devcel.2008.08.020>
- Chiruvella, K. K., Liang, Z., & Wilson, T. E. (2013). Repair of double-strand breaks by end joining. *Cold Spring Harbor Perspectives in Biology*, 5(5). <https://doi.org/10.1101/cshperspect.a012757>
- Cui, Y., Xu, J., Cheng, M., Liao, X., & Peng, S. (2018). Review of CRISPR/Cas9 sgRNA Design Tools. In *Interdisciplinary Sciences – Computational Life Sciences* (Vol. 10, Issue 2, pp. 455–465). Springer. <https://doi.org/10.1007/s12539-018-0298-z>
- Debarnot, V., Kahn, J., & Weiss, P. (2019). Multiview attenuation estimation and correction. *Journal of Mathematical Imaging and Vision*, 61(6), 780–797. <https://doi.org/10.1007/s10851-019-00871-6>

- Dreissig, S., Schiml, S., Schindele, P., Weiss, O., Rutten, T., Schubert, V., Gladilin, E., Mette, M. F., Puchta, H., & Houben, A. (2017). Live-cell CRISPR imaging in plants reveals dynamic telomere movements. *Plant Journal*, *91*(4), 565–573. <https://doi.org/10.1111/tpj.13601>
- Essers, J., Hendriks, R. W., Wesoly, J., Beerens, C. E. M. T., Smit, B., Hoeijmakers, J. H. J., Wyman, C., Dronkert, M. L. G., & Kanaar, R. (2002). Analysis of mouse Rad54 expression and its implications for homologous recombination. *DNA Repair*, *1*(10), 779–793. [https://doi.org/10.1016/S1568-7864\(02\)00110-6](https://doi.org/10.1016/S1568-7864(02)00110-6)
- Ettinger, A., & Wittmann, T. (2014). Fluorescence live cell imaging. In *Methods in Cell Biology* (Vol. 123, pp. 77–94). NIH Public Access. <https://doi.org/10.1016/B978-0-12-420138-5.00005-7>
- Gaj, T., Gersbach, C. A., & Barbas, C. F. (2013). ZFN, TALEN, and CRISPR/Cas-based methods for genome engineering. In *Trends in Biotechnology* (Vol. 31, Issue 7, pp. 397–405). NIH Public Access. <https://doi.org/10.1016/j.tibtech.2013.04.004>
- Gallardo-Escárate, C., Álvarez-Borrego, J., Von Brand, E., Dupré, E., & Del Río-Portilla, M. Á. (2007). Relationship between DAPI-fluorescence fading and nuclear DNA content: An alternative method to DNA quantification? *Biological Research*, *40*(1), 29–40. <https://doi.org/10.4067/S0716-97602007000100004>
- Gleditsch, D., Pausch, P., Müller-Esparza, H., Özcan, A., Guo, X., Bange, G., & Randau, L. (2019). PAM identification by CRISPR-Cas effector complexes: diversified mechanisms and structures. *RNA Biology*, *16*(4), 504–517. <https://doi.org/10.1080/15476286.2018.1504546>
- Goodson, H. V., & Jonasson, E. M. (2018). Microtubules and microtubule-associated proteins. *Cold Spring Harbor Perspectives in Biology*, *10*(6). <https://doi.org/10.1101/cshperspect.a022608>
- Guo, T., Feng, Y. L., Xiao, J. J., Liu, Q., Sun, X. N., Xiang, J. F., Kong, N., Liu, S. C., Chen, G. Q., Wang, Y., Dong, M. M., Cai, Z., Lin, H., Cai, X. J., & Xie, A. Y. (2018). Harnessing accurate non-homologous end joining for efficient precise deletion in CRISPR/Cas9-mediated genome editing. *Genome Biology*, *19*(1), 1–20. <https://doi.org/10.1186/s13059-018-1518-x>
- Heim, R., & Tsien, R. Y. (1996). Engineering green fluorescent protein for improved

- brightness, longer wavelengths and fluorescence resonance energy transfer. *Current Biology*, 6(2), 178–182. [https://doi.org/10.1016/S0960-9822\(02\)00450-5](https://doi.org/10.1016/S0960-9822(02)00450-5)
- Hiersemenzel, K., Brown, E. R., & Duncan, R. R. (2013). Imaging large cohorts of single ion channels and their activity. *Frontiers in Endocrinology*, 4(SEP). <https://doi.org/10.3389/fendo.2013.00114>
- Hindul, N. L., Jhita, A., Oprea, D. G., Hussain, T. A., Gonchar, O., Campillo, M. A. M., O'Regan, L., Kanemaki, M. T., Fry, A. M., Hirota, K., & Tanaka, K. (2022). Construction of a human hTERT RPE-1 cell line with inducible Cre for editing of endogenous genes. *Biology Open*, 11(2). <https://doi.org/10.1242/bio.059056>
- Hustedt, N., & Durocher, D. (2017). The control of DNA repair by the cell cycle. In *Nature Cell Biology* (Vol. 19, Issue 1, pp. 1–9). Nat Cell Biol. <https://doi.org/10.1038/ncb3452>
- Iliakis, G., Wang, H., Perrault, A. R., Boecker, W., Rosidi, B., Windhofer, F., Wu, W., Guan, J., Terzoudi, G., & Pantelias, G. (2004). Mechanisms of DNA double strand break repair and chromosome aberration formation. *Cytogenetic and Genome Research*, 104(1–4), 14–20. <https://doi.org/10.1159/000077461>
- Ishino, Y., Shinagawa, H., Makino, K., Amemura, M., & Nakamura, A. (1987). Nucleotide sequence of the iap gene, responsible for alkaline phosphatase isoenzyme conversion in *Escherichia coli*, and identification of the gene product. *Journal of Bacteriology*, 169(12), 5429–5433. <https://doi.org/10.1128/jb.169.12.5429-5433.1987>
- Jacobsen, L. B., Calvin, S. A., Colvin, K. E., & Wright, M. J. (2004). FuGENE 6 Transfection Reagent: The gentle power. *Methods*, 33(2), 104–112. <https://doi.org/10.1016/j.ymeth.2003.11.002>
- Jagrić, M., Risteski, P., Martinčić, J., Milas, A., & Tolić, I. M. (2021). Optogenetic control of *prc1* reveals its role in chromosome alignment on the spindle by overlap length-dependent forces. *ELife*, 10, 1–79. <https://doi.org/10.7554/eLife.61170>
- Jiang, F., & Doudna, J. A. (2017). CRISPR-Cas9 Structures and Mechanisms. In *Annual Review of Biophysics* (Vol. 46, pp. 505–529). <https://doi.org/10.1146/annurev-biophys-062215-010822>
- Joung, J. K., & Sander, J. D. (2013). TALENs: A widely applicable technology for targeted genome editing. In *Nature Reviews Molecular Cell Biology* (Vol. 14, Issue 1, pp. 49–55).

Nature Publishing Group. <https://doi.org/10.1038/nrm3486>

- Kapuscinski, J. (1995). DAPI: A DNA-Specific fluorescent probe. *Biotechnic and Histochemistry*, *70*(5), 220–233. <https://doi.org/10.3109/10520299509108199>
- Karvelis, T., Gasiunas, G., Young, J., Bigelyte, G., Silanskas, A., Cigan, M., & Siksnys, V. (2015). Rapid characterization of CRISPR-Cas9 protospacer adjacent motif sequence elements. *Genome Biology*, *16*(1), 1–13. <https://doi.org/10.1186/s13059-015-0818-7>
- Komor, A. C., Kim, Y. B., Packer, M. S., Zuris, J. A., & Liu, D. R. (2016). Programmable editing of a target base in genomic DNA without double-stranded DNA cleavage. *Nature*, *533*(7603), 420–424. <https://doi.org/10.1038/nature17946>
- Kubitscheck, U. (2017). Fluorescence microscopy: from principles to biological applications: second edition. In *Fluorescence Microscopy: From Principles to Biological Applications: Second Edition*. <https://doi.org/10.1002/9783527687732>
- Lambrus, B. G., Daggubati, V., Uetake, Y., Scott, P. M., Clutario, K. M., Sluder, G., & Holland, A. J. (2016). A USP28–53BP1–p53–p21 signaling axis arrests growth after centrosome loss or prolonged mitosis. *Journal of Cell Biology*, *214*(2), 143–153. <https://doi.org/10.1083/JCB.201604054>
- Lichtman, J. W., & Conchello, J. A. (2005). Fluorescence microscopy. In *Nature Methods* (Vol. 2, Issue 12, pp. 910–919). Nature Publishing Group. <https://doi.org/10.1038/nmeth817>
- Logan, G., & McCartney, B. (2020). Comparative analysis of taxol-derived fluorescent probes to assess microtubule networks in a complex live three-dimensional tissue. *Cytoskeleton*, *77*(5–6), 229–237. <https://doi.org/10.1002/cm.21599>
- Longo, P. A., Kavran, J. M., Kim, M. S., & Leahy, D. J. (2014). Single cell cloning of a stable mammalian cell line. In *Methods in Enzymology* (Vol. 536, pp. 165–172). Academic Press. <https://doi.org/10.1016/B978-0-12-420070-8.00014-3>
- Ludueña, R. F. (2013). A hypothesis on the origin and evolution of tubulin. In *International Review of Cell and Molecular Biology* (Vol. 302, pp. 41–185). Int Rev Cell Mol Biol. <https://doi.org/10.1016/B978-0-12-407699-0.00002-9>
- Musacchio, A., & Desai, A. (2017). A molecular view of kinetochore assembly and function. In *Biology* (Vol. 6, Issue 1, p. 5). Multidisciplinary Digital Publishing Institute. <https://doi.org/10.3390/biology6010005>

- Nishimasu, H., Ran, F. A., Hsu, P. D., Konermann, S., Shehata, S. I., Dohmae, N., Ishitani, R., Zhang, F., & Nureki, O. (2014). Crystal structure of Cas9 in complex with guide RNA and target DNA. *Cell*, *156*(5), 935–949. <https://doi.org/10.1016/j.cell.2014.02.001>
- Novak, M., Polak, B., Simunić, J., Boban, Z., Kuzmić, B., Thomae, A. W., Tolić, I. M., & Pavin, N. (2018). The mitotic spindle is chiral due to torques within microtubule bundles. *Nature Communications*, *9*(1), 1–10. <https://doi.org/10.1038/s41467-018-06005-7>
- Papini, D., Levasseur, M. D., & Higgins, J. M. G. (2021). The Aurora B gradient sustains kinetochore stability in anaphase. *Cell Reports*, *37*(6), 109818. <https://doi.org/10.1016/j.celrep.2021.109818>
- Parker, A. L., Teo, W. S., Pandzic, E., Vicente, J. J., McCarroll, J. A., Wordeman, L., & Kavallaris, M. (2018).  $\beta$ -Tubulin carboxy-terminal tails exhibit isotype-specific effects on microtubule dynamics in human gene-edited cells. *Life Science Alliance*, *1*(2). <https://doi.org/10.26508/lsa.201800059>
- Picot, J., Guerin, C. L., Le Van Kim, C., & Boulanger, C. M. (2012). Flow cytometry: Retrospective, fundamentals and recent instrumentation. In *Cytotechnology* (Vol. 64, Issue 2, pp. 109–130). Springer. <https://doi.org/10.1007/s10616-011-9415-0>
- Polak, B., Risteski, P., Lesjak, S., & Tolić, I. M. (2017). PRC 1-labeled microtubule bundles and kinetochore pairs show one-to-one association in metaphase. *EMBO Reports*, *18*(2), 217–230. <https://doi.org/10.15252/embr.201642650>
- Prasher, D. C., Eckenrode, V. K., Ward, W. W., Prendergast, F. G., & Cormier, M. J. (1992). Primary structure of the *Aequorea victoria* green-fluorescent protein. *Gene*, *111*(2), 229–233. [https://doi.org/10.1016/0378-1119\(92\)90691-H](https://doi.org/10.1016/0378-1119(92)90691-H)
- Qi, L. S., Larson, M. H., Gilbert, L. A., Doudna, J. A., Weissman, J. S., Arkin, A. P., & Lim, W. A. (2013). Repurposing CRISPR as an RNA-guided platform for sequence-specific control of gene expression. *Cell*, *152*(5), 1173–1183. <https://doi.org/10.1016/j.cell.2013.02.022>
- Ran, F. A., Hsu, P. D., Wright, J., Agarwala, V., Scott, D. A., & Zhang, F. (2013). Genome engineering using the CRISPR-Cas9 system. *Nature Protocols*, *8*(11), 2281–2308. <https://doi.org/10.1038/nprot.2013.143>
- Remington, S. J. (2011). Green fluorescent protein: A perspective. In *Protein Science* (Vol. 20,

Issue 9, pp. 1509–1519). John Wiley & Sons, Ltd. <https://doi.org/10.1002/pro.684>

- Sanderson, M. J., Smith, I., Parker, I., & Bootman, M. D. (2014). Fluorescence microscopy. *Cold Spring Harbor Protocols*, 2014(10), 1042–1065. <https://doi.org/10.1101/pdb.top071795>
- Schmid-Burgk, J. L., Höning, K., Ebert, T. S., & Hornung, V. (2016). CRISPaint allows modular base-specific gene tagging using a ligase-4-dependent mechanism. *Nature Communications* 2016 7:1, 7(1), 1–12. <https://doi.org/10.1038/ncomms12338>
- Scott, S. J., Suvarna, K. S., & D'Avino, P. P. (2020). Synchronization of human retinal pigment epithelial-1 cells in mitosis. *Journal of Cell Science*, 133(18). <https://doi.org/10.1242/jcs.247940>
- Smoak, E. M., Stein, P., Schultz, R. M., Lampson, M. A., & Black, B. E. (2016). Long-term retention of CENP-A nucleosomes in mammalian oocytes underpins transgenerational inheritance of centromere identity. *Current Biology*, 26(8), 1110–1116. <https://doi.org/10.1016/j.cub.2016.02.061>
- Štimac, V., Koprivec, I., Manenica, M., Simunić, J., & Tolić, I. M. (2022). Augmin prevents merotelic attachments by promoting proper arrangement of bridging and kinetochore fibers. *ELife*, 11, 83287. <https://doi.org/10.7554/elife.83287>
- Svalastog, A. L., & Martinelli, U. (2013). Representing life as opposed to being: The bio-objectification process of the hela cells and its relation to personalized medicine. *Croatian Medical Journal*, 54(4), 397–402. <https://doi.org/10.3325/cmj.2013.54.397>
- Tolić, I. M. (2018). Mitotic spindle: kinetochore fibers hold on tight to interpolar bundles. *European Biophysics Journal*, 47(3), 191–203. <https://doi.org/10.1007/s00249-017-1244-4>
- Tsien, R. Y. (1998). The green fluorescent protein. In *Annual Review of Biochemistry* (Vol. 67, pp. 509–544). <https://doi.org/10.1146/annurev.biochem.67.1.509>
- Valdivia, M., Hamdouch, K., Ortiz, M., & Astola, A. (2009). CENPA a genomic marker for centromere activity and human diseases. *Current Genomics*, 10(5), 326–335. <https://doi.org/10.2174/138920209788920985>
- Vanpoeringhe, L., Carlier-Grynkor, F., Cornilleau, G., Kusakabe, T., Drinnenberg, I. A., & Tran, P. T. (2021). Live-cell imaging reveals square shape spindles and long mitosis

- duration in the silkworm holocentric cells. *MicroPublication Biology*, 2021. <https://doi.org/10.17912/micropub.biology.000441>
- Vicidomini, G., Bianchini, P., & Diaspro, A. (2018). STED super-resolved microscopy. In *Nature Methods* (Vol. 15, Issue 3, pp. 173–182). <https://doi.org/10.1038/nmeth.4593>
- Wade, R. H. (2009). On and around microtubules: An overview. In *Molecular Biotechnology* (Vol. 43, Issue 2, pp. 177–191). Springer. <https://doi.org/10.1007/s12033-009-9193-5>
- Walczak, C. E., & Heald, R. (2008). Mechanisms of mitotic spindle assembly and function. In *International Review of Cytology* (Vol. 265, pp. 111–158). Academic Press. [https://doi.org/10.1016/S0074-7696\(07\)65003-7](https://doi.org/10.1016/S0074-7696(07)65003-7)
- Walss-Bass, C., Xu, K., David, S., Fellous, A., & Ludueña, R. F. (2002). Occurrence of nuclear  $\beta$ II-tubulin in cultured cells. *Cell and Tissue Research*, 308(2), 215–223. <https://doi.org/10.1007/s00441-002-0539-6>
- Wiesenhofer, B., & Humpel, C. (2000). Lipid-mediated gene transfer into primary neurons using FuGene: Comparison to C6 glioma cells and primary glia. *Experimental Neurology*, 164(1), 38–44. <https://doi.org/10.1006/exnr.2000.7414>
- Wirth, R., Gao, P., Nienhaus, G. U., Sunbul, M., & Jäschke, A. (2019). SiRA: a silicon rhodamine-binding aptamer for live-cell super-resolution RNA imaging. *Journal of the American Chemical Society*, 141(18), 7562–7571. <https://doi.org/10.1021/jacs.9b02697>
- Xu, Y., & Li, Z. (2020). CRISPR-Cas systems: Overview, innovations and applications in human disease research and gene therapy. In *Computational and Structural Biotechnology Journal* (Vol. 18, pp. 2401–2415). Research Network of Computational and Structural Biotechnology. <https://doi.org/10.1016/j.csbj.2020.08.031>
- Ying, Z., Yang, J., Li, W., Wang, X., Zhu, Z., Jiang, W., Li, C., & Sha, O. (2020). Astrin: a key player in mitosis and cancer. In *Frontiers in Cell and Developmental Biology* (Vol. 8, p. 866). Frontiers Media SA. <https://doi.org/10.3389/fcell.2020.00866>
- Yu, K., Liu, C., Kim, B. G., & Lee, D. Y. (2015). Synthetic fusion protein design and applications. *Biotechnology Advances*, 33(1), 155–164. <https://doi.org/10.1016/j.biotechadv.2014.11.005>

WEB: <https://www.fpbases.org/protein/taggfp2/> date accessed: 2023-01-12



## 8. Curriculum vitae

I was born in Zagreb, Croatia, where I finished elementary school and general gymnasium. In 2017, I was admitted in the Undergraduate Degree program in Molecular Biology at the Faculty of Science, University of Zagreb. During my undergraduate studies, I participated in a science popularization event 'Biology Night' two years in a row and in 2018, I was a student teaching assistant on a zoology course. In the summer of 2019, I went on a CEEPUS student exchange in Slovenia where I worked on a project at the Faculty of Health Sciences, University of Ljubljana. In 2020, enrolled in the Masters Degree program in Molecular Biology at the same faculty. Later that year, I did laboratory practice in the Laboratory for Hereditary Cancer, Ruđer Bošković Institute, Zagreb. During master's studies I was a member of Biology Students Association – BIUS and I participated in their activities. I was also on the faculty's rowing team for the past five years and I represented my faculty and the university on several rowing competitions in Croatia.

### **Publications:**

Bohinc, K., **Tintor, E.**, Kovačević, D., Vidrih, R., Zore, A., Abram, A., Kojić, Ž., Obradović, M., Veselinović V. & Dolić, O. (2021). Bacterial Adhesion on Glass–Ionomer Cements and Micro/Nano Hybrid Composite Dental Surfaces. *Coatings*, 11(2), 235